

Distribution Agreement

In presenting this thesis or dissertation as a partial fulfillment of the requirements for an advanced degree from Emory University, I hereby grant to Emory University and its agents the non-exclusive license to archive, make accessible, and display my thesis or dissertation in whole or in part in all forms of media, now or hereafter known, including display on the world wide web. I understand that I may select some access restrictions as part of the online submission of this thesis or dissertation. I retain all ownership rights to the copyright of the thesis or dissertation. I also retain the right to use in future works (such as articles or books) all or part of this thesis or dissertation.

Signature:

Kevin Z. Chen

Date

Modulating Mitofusins to Enhance Therapeutic T Cell Expansion and Persistence

By
Kevin Z. Chen
Master of Science

Graduate Division of Biological and Biomedical Science
Cancer Biology

Edmund K. Waller, MD, PhD, FACP
Advisor

Curtis J. Henry, PhD
Committee Member

Richard A. Kahn, PhD
Committee Member

Accepted:

Kimberly Jacob Arriola PhD, MPH
Dean of the James T. Laney School of Graduate Studies

Date

Modulating Mitofusins to Enhance Therapeutic T Cell Expansion and Persistence

By
Kevin Z. Chen
B.S., University of Maryland – Baltimore County, 2019

Advisors:
Edmund K. Waller, MD, PhD, FACP

An abstract of

A thesis submitted to the Faculty of the James T. Laney School of Graduate Studies of Emory University in partial fulfillment of the requirements for the degree of Master of Science in the Graduate Division of Biological and Biomedical Science, Cancer Biology, 2022.

Abstract

Modulating Mitofusins to Enhance Therapeutic T Cell Expansion and Persistence By Kevin Z. Chen

Chronic lymphocytic leukemia (CLL), a cancer of B-lymphocytes, is the most common leukemia in adults. While current frontline therapies for CLL, such as ibrutinib or a combination of venetoclax and obinutuzumab, have significantly improved clinical outcomes for patients with treatment-naïve CLL and relapsed and refractory CLL (RR-CLL), complete response (CR) rates for RR-CLL patients on ibrutinib remain between 5-14%. However, with the advent of chimeric antigen receptor T cells (CART), CR rates for RR-CLL are increased to around 26-29%, which is in sharp contrast to the 70-93% CR rates achieved using CART to treat patients with B-cell acute lymphoblastic leukemia (B-ALL). This discrepancy in response rates is due, in part, to the inherently immunosuppressive nature of CLL. In addition, T cells from CLL patients are significantly deficient in CD8 co-receptor expressing (CD8+) T cells, including naïve T (Tn), stem cell-like memory T (Tscm), and central memory T (Tcm) cells. Thus, elucidating translatable mechanisms for selective expansion of Tn, Tscm and Tcm from CLL patients is needed to improve the efficacy of CART cell therapy for CLL patients.

To that end, members of our lab have demonstrated that dual inhibition of Phosphoinositide 3-Kinase (PI3K) δ/γ isoforms with IPI-145 (duvelisib) preferentially expands CD8⁺ T cells, including Tn, Tscm and Tcm, as well as improves the *in vivo* persistence and cytotoxicity of CD19-targeted CART (CD19-CART). Furthermore, my immunoblot analysis of T cells cultured with duvelisib for 15 days reveals increases in the expression of epigenetic and transcriptional regulators of memory T cell programs, including sirtuins 1/3/5, FOXO1/3, TCF1/7, and ID3. In addition, *ex vivo* duvelisib treatment of CLL patient T cells increased expression of essential mitochondrial fusion proteins, mitofusins 1 and 2 (MFN1/2), and decreased serine 637 phosphorylation, and thereby inactivation, of mitochondrial fission protein, DRP1, both consistent with an increase in mitochondrial fusion. Interestingly, duvelisib increased the spare respiratory capacity of CD8⁺ T cells but did not alter the average mitochondrial cross-sectional area of bulk T cells, assessed by extracellular flux analysis and transmission electron microscopy (TEM), respectively. These data, taken together, demonstrate intersections between PI3K δ/γ inhibition, mitochondrial fusion, and T cell memory. However, as modulating PI3K signaling affects many downstream processes in T cell biology, duvelisib may not increase T cell expansion uniformly across all CLL patient samples.

Given the potential role of mitochondrial fusion in enhancing Tn/Tscm and Tcm persistence and function, I devised an alternative approach to PI3K δ/γ dual inhibition to induce mitochondrial fusion pharmacologically. Using the first-in-class mitofusin activating small molecule, MASM7, I sought to enhance MFN1/2 activity in CLL patient T cells. My data demonstrate that T cell cultures treated with MASM7 doses between 100nM - 250nM daily for nine days have >50% more CD8⁺ and CD8⁺CD27⁺CD45RO⁻ T cells, compared to duvelisib and vehicle control groups. In addition, MASM7 induces significant increases in mitochondrial volume per mitochondrion and mitochondrial membrane potential to mass ratios, indicative of enhanced mitochondrial fusion. Interestingly, T cells treated with MASM7 do not exhibit increased MFN1/2 expression. However, further studies are required to confirm suggested changes in expression of biomarkers for T cell activation (TIM-3, PD-1, and LAG-3), proliferation (Ki-67), and self-renewal (TCF1).

In conclusion, I have shown that either dual inhibition of Phosphoinositide 3-Kinase (PI3K) δ/γ with IPI-145 (duvelisib) or MFN1/2 agonism with MASM7 improved the *ex vivo* expansion of CLL patient T cells. Further characterization of both strategies is required to confirm the cytotoxicity of MASM7-expanded CART, more definitively establish the mechanisms of action for duvelisib and MASM7, and determine potential synergy between duvelisib and MASM7 during *ex vivo* T cell expansion and CART generation, with predicted improved outcomes among CLL patients.

Acknowledgements

I would first like to thank my advisor, Dr. Edmund Waller, for his expertise and guidance throughout my research and training. Your insight in the complexities of cancer immunology were indispensable to the completion of my thesis research.

I would also like to thank Dr. Malathy Shanmugam and Dr. Evripidis Gavathiotis for their expert guidance on the interrogation of cancer and mitochondrial metabolism. I thank Dr. Aditi Sharma from the Shanmugam lab for patiently training me in the basics of metabolic flux analysis and Dr. Emmanouil Zacharioudakis from the Gavathiotis lab for assisting in the careful design of all experiments related to the interrogation of MASM7 as a novel mitofusin agonist.

I extend my most sincere gratitude to my thesis committee members, Drs. Curtis Henry and Richard Kahn for their expertise and supportive mentorship during my graduate research and completion of this thesis.

In addition, I would like to thank Drs. Chrystal Paulos, Sunil Raikar, and Jean Koff for their guidance and collaboration on key aspects of my thesis research.

Moreover, I would like to thank Drs. Gaurav Joshi, Ricardo Guerrero-Ferreira, and Ms. Jeannette Taylor for their technical expertise and assistance in the widefield, SIM, and electron microscopy experiments described in this body of research.

I thank my fellow lab members and Cancer Biology Graduate Program Peers for engaging me in invigorating discussions and providing integral assistance in the design and execution of the experiments described herein. Of note, I thank my colleagues, Passang, Ronnie Funk, and Shuhua Wang for their contributions to this thesis work.

Finally, I would like to thank my family members and Dennis Elias for their unwavering support and love, including during the completion of my thesis.

List of Abbreviations and Terms

Abbreviation	Definition
3D-SIM	3D-Structured Illumination Microscope/Microscopy
B-ALL	B-cell Acute Lymphoblastic Leukemia
CART	Chimeric Antigen Receptor T cell
CD19-CART	CD19 antigen-targeted Chimeric Antigen Receptor T cells
CD8+	CD8 co-receptor expressing
CLL	Chronic Lymphocytic Leukemia
duv-T/CART	Duvelisib-treated T cells or duvelisib-treated CD19-CART
DRP1	Dynamin-related protein 1; GTPase that promotes mitochondrial fission
ECAR	Extracellular Acidification Rate
ETC	Electron Transport Chain
FAO	Fatty Acid Oxidation
IMM	Inner mitochondrial membrane
Ki-67	Antigen KI-67; nuclear protein that is associated with cellular proliferation
LAG-3	Lymphocyte Activation Gene 3; CD223
MASM7	Mitofusin Activating Small Molecule 7
MFN1/2	Mitofusins 1 and 2; GTPases that promotes mitochondrial outer membrane fusion
NOG	NOD/Shi-scid/IL-2R γ null mouse; severely immunodeficient mouse
OCR	Oxygen Consumption Rate
OMM	Outer mitochondrial membrane
OPA1	Optic Atrophy 1; GTPase that promotes mitochondrial inner membrane fusion
OSU-CLL	Ohio State University-Chronic Lymphocytic Leukemia; cell line
OXPHOS	Oxidative Phosphorylation
PD-1	Programmed cell Death protein 1; CD279
PGC1a	Protein encoded by the PPARGC1A gene; promotes mitochondrial biogenesis
PI3K δ/γ	Phosphoinositide 3-kinase delta and gamma isoforms
RR-	Relapsed and Refractory-
SIRT	Sirtuin; NAD ⁺ -dependent deacetylases (i.e. SIRT1/3) and deacylases (i.e. SIRT5)
TCF1	T cell factor 1; T-cell-specific transcription factor
Tcm	Central Memory T cell
Tem	Effector Memory T cell
TEM	Transmission Electron Microscope/Microscopy
Temra/Tte	Effector Memory CD45RA-expressing T cell/Terminal Effector T cell
TIM-3	T cell Immunoglobulin and Mucin domain-containing protein 3; CD366
TMRM	Tetramethylrhodamine, methyl ester; readily sequestered by active mitochondria
Tn	Naïve T cell
Tscm	Stem Cell-like Memory T cell

Term	Definition
CART manufacture	Generation of Chimeric Antigen Receptor T cells from patient-derived T cells
Expansion	Increase in total T cell number due to replication and division existing T cells
Persistence	Sustained prevalence of total or subset-specific T cells
Mitotracker	Fluorescent dyes used to assess mitochondrial mass and membrane potential
Untreated	No previous treatment with chemotherapeutic agent(s) prior to sample donation
Pre-treated	Ongoing treatment with chemotherapeutic agent(s) at the time of sample donation

Table of Contents

Introduction

The therapeutic value of cart cell therapy in hematological malignancies	1
Discrepancies in response to cart therapy	1-2
Inhibition of PI3K δ/γ isoforms in the in vivo persistence and cytotoxicity of CD19-CART	2
Mitochondrial fusion and OXPHOS are required for the maintenance of T cell memory	3
Molecular structure of Mitofusin 1 and 2	3-4
Mitochondrial dynamics in cellular homeostasis and disease	4-5
MASM7 is a first-in-class direct activator of MFN1/2	5-9
Research Summary	10-12

Results

Inhibition of PI3K δ/γ favors mitofusin expression and activity	13-15
Electron imaging suggests inhibition of PI3K δ/γ favors fusion	16-17
Differences in mitochondrial quality between patients may predict response to duvelisib	17-25
Duvelisib induced pathways converge on MFN1/2	25-30
MASM7 promotes CD8+ T cell expansion and mitochondrial fusion	30-34

Discussion 35-36

Closing Remarks 37

Materials and Methods

Materials	38-41
Sample Collection, Leukapheresis, and PBMC isolation	42
T-cell activation and expansion	42-43
CART experiments	43
Flow Cytometry	43-44
Seahorse Assay	44
Immunoblot/Western Blot	44-45
Immunofluorescent Staining for Widefield Imaging	45-46
Statistical analysis	46
Protocol 1: Mitochondrial Mass and Membrane Potential Staining for Human Lymphocytes	47
Protocol 2: Immunoblot/Western Blot Protocol	48-49

Works Cited 50-54

List of Figures

Figure 1. B-CLL patients have fewer CD8 ⁺ CD27 ⁺ CD45RO ⁻ naïve T cells.	1
Figure 2. duv-CART conferred a survival advantage in B-CLL bearing mice.	2
Figure 3. Mitofusin structure and <i>trans</i> -dimerization initiates mitochondrial fusion.	4
Figure 4. Schematic depicting MFN1/2 activation by MASM7.	7
Figure 5. Experimental workflow for <i>in vitro</i> studies.	9
Figure 6. PI3K δ/γ dual inhibition with duvelisib and MFN1/2 activation with MASM7 converge to promote T _n /T _{cm} expansion and persistence.	12
Figure 7. Regulators of mitochondrial dynamics are differentially affected by inhibition of PI3K δ/γ .	15
Figure 8. TEM images suggests that duvelisib does not increase mitochondrial fusion.	17
Figure 9. Duvelisib does not increase respiratory capacity of untreated CLL patient T cells.	19
Figure 10. Duvelisib favors respiration and glycolytic compensation in healthy donor T cells.	21
Figure 11. Mitochondrial mass and membrane potential of CD4 ⁺ T cells change following prolonged T cell culture irrespective of duvelisib treatment.	24-25
Figure 12. Mitophagy pathways are upregulated in duv-T.	26
Figure 13. Duvelisib induces expression of both apoptotic and anti-apoptotic proteins.	27
Figure 14. Duvelisib favors memory T cell programs.	28
Figure 15. SIRT1 activity and MFN1/2 coincide during prolonged <i>in vitro</i> T cell culture.	29
Figure 16. MASM7 augments T cell expansion.	31
Figure 17. MASM7 does not affect MFN2 expression.	32
Figure 18. MASM7 augments T cell expansion.	33
Figure S1. Duvelisib expands T _{cm} as well as pre-treated CLL and healthy donor T cells	36
Table S1. Table of Human Samples	38
Table S3. Table of Flow Cytometry Reagents	39
Table S3. Table of Western Blot Antibodies	40

Introduction

The Therapeutic Value of CART Cell Therapy in Hematological Malignancies

Despite recent advances using Bruton Tyrosine Kinase, PI3K δ , and B-Cell Lymphoma-2 inhibitors for the treatment of CLL, acquired resistance to these inhibitors remains common.⁷⁻⁹ Moreover, as patient eligibility for allogeneic hematopoietic stem cell transplant is limited by patient age and performance status, CART therapy provides an attractive option for CLL patients.¹⁰ CARTs are patient-derived T cells that are genetically engineered to express chimeric receptors that recognize specific cancer cell surface antigens, such as the CD19 protein overexpressed on malignant B cells.¹¹ Upon receptor activation, CD19-CART degranulate to induce CLL cell death through the release of cytotoxic granules containing lytic proteins, such as perforins and granzymes. To date, the FDA has approved four autologous T cell products genetically engineered to express CD19-targeting CARs for the treatment of diffuse large B cell lymphoma, B-ALL, mantle cell lymphoma, and follicular lymphoma.¹²⁻¹⁵

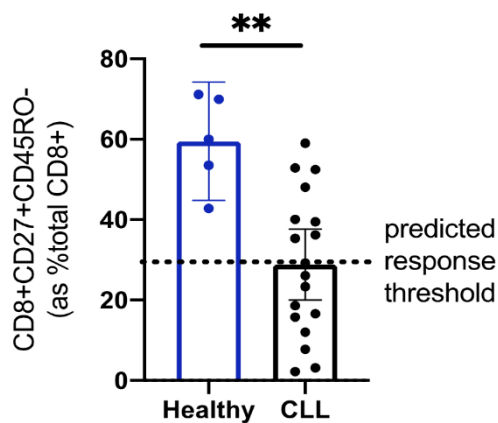


Figure 1. B-CLL patients have fewer CD8+CD27+ CD45RO- naïve T cells.¹ Total T cell populations isolated from B-CLL patient and healthy donor whole blood were analyzed by FACS. The fraction of CD8+CD27+CD45RO- T cells is plotted as a percentage of total CD8+ T cells. The predicted response threshold is labeled as a dotted line.

Discrepancies in Response to CART Therapy

Studies have identified several key obstacles in the pre-clinical to clinical translation of CART therapies, including heterogeneous expression of target antigens, loss of target antigen expression, lack of T cell persistence following infusion, and extensive T cell exhaustion in the immunosuppressive leukemic or tumor microenvironment.¹⁶⁻¹⁹ Previous work that correlated T cell phenotype with CART efficacy in CLL patients found that a threshold frequency of more than 29% of CD8+CD27+CD45RO- naïve T cells in blood prior to CART manufacturing predicted complete responses to

CART therapy.²⁰ My lab has shown that T cells from Rai Stage 0-1 CLL patients have fewer CD8+CD27+CD45RO- naïve T cells compared to healthy donors, with over half of CD8+ T cells falling below the threshold frequency predictive of response ($p < 0.005$; **Figure 1**).¹ Thus, expanding naïve and central memory T cell subsets *ex vivo* is key to improving response to CART therapy.

Inhibition of PI3K δ/γ isoforms in the *in vivo* persistence and cytotoxicity of CD19-CART

Members of my lab have shown that addition of duvelisib, a dual inhibitor of PI3K δ/γ subunits, to *ex vivo* T cell or CART cultures increases the proportion of CD8+ cells, including naïve (Tn), stem cell-like memory (Tscm), and central memory (Tcm) subsets.¹ Duvelisib treated T cells (duv-T) also have decreased expression of activation markers TIM3, LAG3, and PD1.¹ In contrast, simultaneous co-expression of TIM3, LAG3, and PD1 on tumor infiltrating lymphocytes have been linked to T cell exhaustion and poor disease prognosis.^{1, 21-23} Following transfer to immunodeficient (NOG) mice engrafted with a human CLL cell line (OSU-CLL), duvelisib-expanded CART (duv-CART) cells demonstrated robust *in vivo* expansion, faster elimination of OSU-CLL (**Figure 2A**), longer persistence ($p < 0.0005$; **Figure 2B**), and significantly improved survival among CLL-bearing mice following CART therapy ($p < 0.005$; **Figure 2C**). However, PI3K signaling affects many aspects of T cell

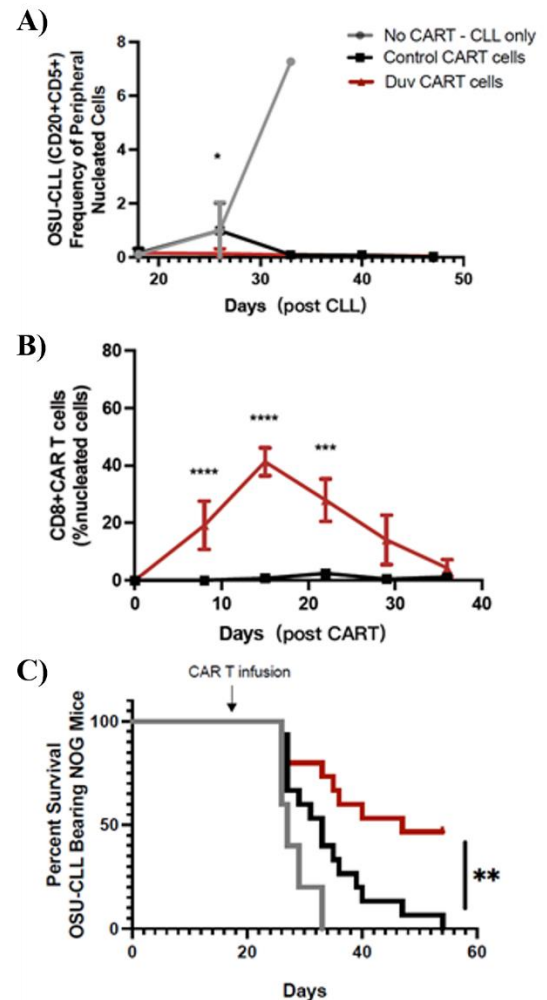


Figure 2. duv-CART conferred a survival advantage in B-CLL bearing mice.¹ OSU-CLL engrafted NOG mice were treated with 1×10^6 control- or duv-CART on day 15. CART efficacy was assessed by flow for A) frequency of CD20+CD5+ OSU-CLL in blood, B) CD8+ CART cells in blood following infusion, and C) Kaplan-Meier survival analysis of treated mice. ** $p < 0.005$, * $p < 0.05$

biology and the mechanisms underlying duvelisib's effect on T cell expansion are unknown. Despite significant increases in the relative proportion and total numbers of CD8+ T cells during *ex vivo* expansion, the effect of duvelisib is highly variable between patient samples (data not shown). Thus, identifying more direct methods of consistently expanding patient T cells is paramount.

Mitochondrial Fusion and OXPHOS are Required for the Maintenance of T Cell Memory

Following antigen clearance and T cell contraction, only long-lived central memory T cells (Tcm) retain the ability to rapidly differentiate into effector T cells upon secondary antigen exposure. Increased fatty acid oxidation (FAO), oxidative phosphorylation (OXPHOS), and mitochondrial fusion are associated with increased persistence of Tcm.^{24, 25} Furthermore, mitochondrial fusion leads to the tightening of cristae and the close association of neighboring electron transport chain (ETC) complexes, producing conditions that favor efficient OXPHOS and Tcm development.^{24, 26} The Pearce group has shown that overexpression of OPA1 increases mitochondrial fusion and supports Tcm development without regulating FAO.²⁴ Importantly, genetic deletion of OPA1, MFN1, or MFN2 impairs efficient OXPHOS.²⁴ However, the contribution of MFNs to utilization of the FAO pathway and Tcm development is unclear. A number of studies have revealed important roles for MFNs in maintaining hematopoietic progenitor cells with the potential for extensive lymphoid differentiation and expansion and enhancing CD4+ T cell function.²⁷⁻²⁹ Early on in my thesis research, I found that MFNs are upregulated in bulk CD3+ T cells following duvelisib treatment, furthering our existing interest in mitochondrial morphology and metabolism as key regulators of T cell function.¹

Molecular structure of Mitofusin 1 and 2

MFN1 and MFN2 proteins share high sequence homology. Both homologs contain a N-terminal GTPase domain, a coiled-coiled heptad repeat (HR1) domain, a transmembrane domain, and a C-terminal HR2 domain. A proline rich region is exclusive to MFN2 (Figure 3).³⁰ MFN1/2 are essential for the tethering of

adjacent mitochondria and execution of outer mitochondrial membrane (OMM) fusion. Mitochondrial tethering requires MFN2-MFN2 homo- or MFN2-MFN1 hetero-dimerization at HR2 and GTPase domains (Figure 3B).^{31, 32} Prior to fusion, intramolecular HR1-HR2 interactions position mitofusins in an anti-tethering conformation that prevents fusion (Figure 3A). During fusion, HR2 is released from HR1 to position mitofusins in a pro-tethering conformation and allow for *trans*-dimerization of MFN2-MFN2 or MFN2-MFN1 (Figure 3B). Thus, an inhibitor of intramolecular HR1-HR2 interactions could maintain MFN1/2 in a conformationally active state.

Mitochondrial dynamics in cellular homeostasis and disease

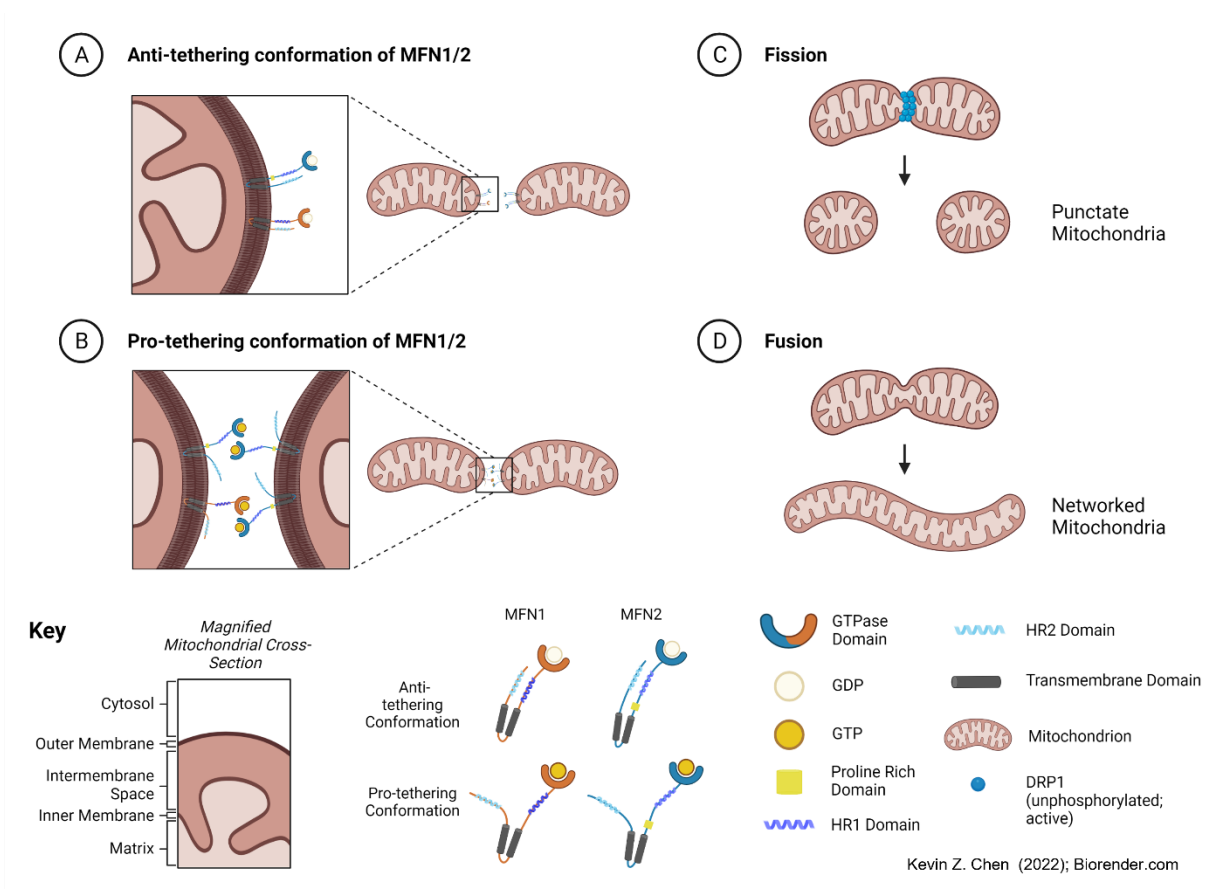


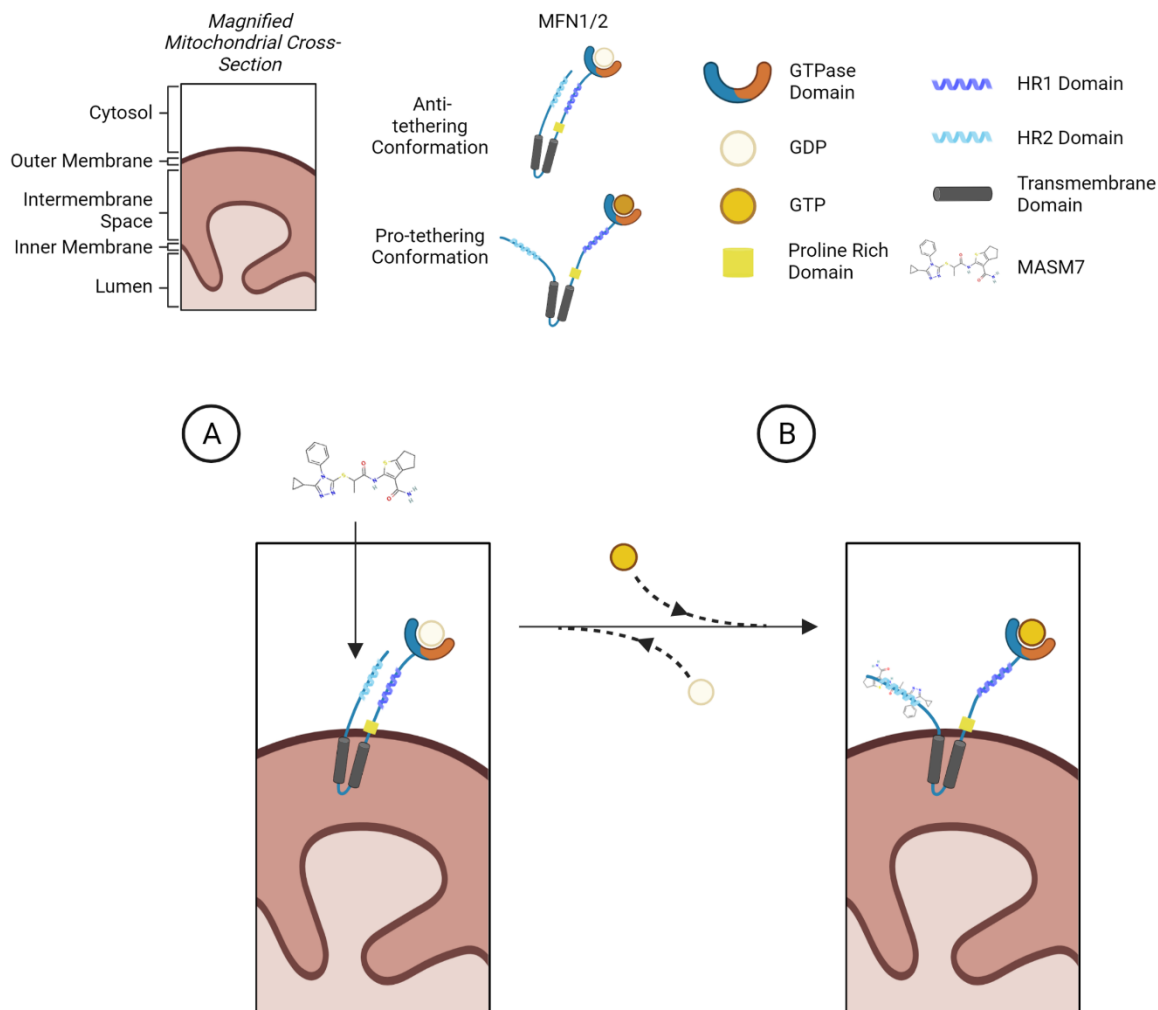
Figure 3. Mitofusin structure and *trans*-dimerization initiates mitochondrial fusion. Graphical depiction of A) MFN1 (orange) and MFN2 (teal) in the anti-tethering conformation, B) MFN2-MFN2 and MFN1-MFN2 *trans*-dimerization of MFN1/2 in the pro-tethering conformation, C) Mitochondrial fission mediated by DRP1 to form punctate mitochondria, and D) Mitochondrial fusion mediated by MFN1/2 on the outer mitochondrial membrane and OPA1 on the inner mitochondrial membrane (not depicted). The key for all structural elements is shown at the bottom. Structural elements are not drawn to scale.

Mitochondria are central for generating bioenergy, biosynthesis of precursors for duplication of biomass and maintenance of redox homeostasis, and regulators of autophagy and cell death. The aforementioned processes are regulated by dynamic networks of mitochondria that present four distinct morphologies: punctate, rod-like, networked, and round and large.³³ Fission or fragmentation of a networked mitochondrion produces morphologically fragmented or punctate mitochondria (Figure 3C), while fusion generates elongated networks of mitochondria (Figure 3D). Formation of these mitochondrial networks are

governed by mitochondrial fission and fusion. Dynamin-related protein 1 (DRP1) is a cytosolic GTP hydrolase (GTPase) that is recruited to the OMM to mediate fission, generating fragmented and punctate mitochondria. Mitochondrial fission plays a role in diverse cell fates, including facilitating mitophagy, accelerating cell proliferation, and mediating apoptosis. In contrast, mitochondrial fusion is mediated by the GTPases, MFN1/2 in the OMM and optic atrophy 1 (OPA1) in the inner mitochondrial membrane (IMM). To increase the longevity of aged/dysfunctional mitochondria, healthy mitochondria fuse to damaged mitochondria, exchanging intact mitochondrial DNA (mtDNA) copies. Mitochondrial fusion increases electron transport chain (ETC) protein complex density and enhances physical links between mitochondria and the endoplasmic reticulum, interactions which are important for calcium ion flux. Importantly, inhibition of mitochondria fusion or loss of MFN1 or MFN2 lead to a reduction in mtDNA stability and copy number due to defects in mitochondrial complementation. While MFN1 and MFN2 have some functional redundancy, MFN1, but not MFN2, is required for OPA1-initiated mitochondrial fusion.³⁴ Additionally, mutation and dysfunction of MFN2, but not MFN1 or OPA1, prevents effective mitochondrial fusion and has been implicated in Charcot-Marie-Tooth disease type 2A, Alzheimer's disease, obesity, diabetes, and cancer.

MASM7 is a first-in-class direct activator of MFN1/2

Despite the growing evidence that mitochondrial fusion is important for T cell stemness and function, direct activation of mitochondrial fusogens in therapeutic T cell products has not been explored. The series of mitofusin activating small molecules (MASMs) characterized by the Gavathiotis group at Albert Einstein College of Medicine represents the first small molecules capable of directly inducing the conformational activation of MFN1/2.³⁵ Of the 18 candidate MASMs that were selected from an *in silico* screen of over 13.8×10^6 commercially available small molecules, MASM7, in particular, exhibits specific binding to the HR2 domain with high specificity to disrupt HR1-HR2 interaction, enforces the pro-tethering conformation of MFN1/2, and promotes mitochondrial fusion.³⁵



Kevin Z. Chen (2022); Biorender.com

Figure 4. Schematic depicting MFN1/2 activation by MASM7. After entering the cell, MASM7 A) binds to the HR2 domain of MFN1/2 present on the outer mitochondrial membrane to disrupt HR1-HR2 interaction and prevents the HR2 domain of MFN1/2 from forming the anti-tethering conformation with the HR1 domain of MFN1/2. As a result, MASM7 B) directly activates MFN1/2 by inducing the pro-tethering conformation of MFN1/2. GDP/GTP exchange within the GTPase domain of MFN1/2 is also depicted in between A) and B).

MASM7 (CAS#920868-45-7) is a synthetic compound synthesized by Enamine, Ltd. While the biological activity, half-life, availability, and reactivity of MASM7 are not well characterized, MASM7 is known to

be stable at ambient temperature as a solid beige powder with a melting point of 167°C. Based on the *in silico* pharmacophore model of MFN1/2, consisting of three hydrophobic groups, an aromatic ring, and a hydrogen bond donor, MASM7 is predicted to mimic the residues within the HR1 domain and bind to the HR2 domain of MFN1/2 with high specificity (Figure 4A). By occupying the residues within the HR2 domain responsible for autoinhibitory interaction of the HR1 and HR2 domains, MASM7 maintains MFN1/2 in an “open” or pro-tethering conformation (Figure 4B). Thus, MASM7 competitively binds to the HR2 domain, prevents the HR1 domain from interacting with the HR2 domain in an anti-tethering conformation, and directly promotes MFN1- or MFN2-mediated fusion.

Preliminary studies indicate that MASM7 potently induces mitochondrial fusion in wild-type (WT) mouse embryonic fibroblasts (MEFs) ($EC_{50} = 75\text{nM}$).³⁵ While genetic knockout of MFN1 or MFN2 in MEFs reduces the capacity of MASM7 to promote mitochondrial fusion, MASM7 does not promote fusion in MFN1/2 double knockout MEFs. However, MASM7 retains the capacity to induce mitochondrial fusion in DRP1 knockout MEFs. Taken together, these data suggest that MASM7 directly activates MFN1 or MFN2 to promote fusion and excludes the possibility MASM7 inhibits DRP1, a mitochondrial fission protein, as a mechanism of fusion enhancement.³⁵ Although MAMS7 had not previously been studied in the context of human lymphocyte culture, I hypothesized that investigating MASM7 as a potential T cell expansion reagent would greatly inform our understanding of the role of MFN1/2 in expansion and persistence of memory T cell subsets.

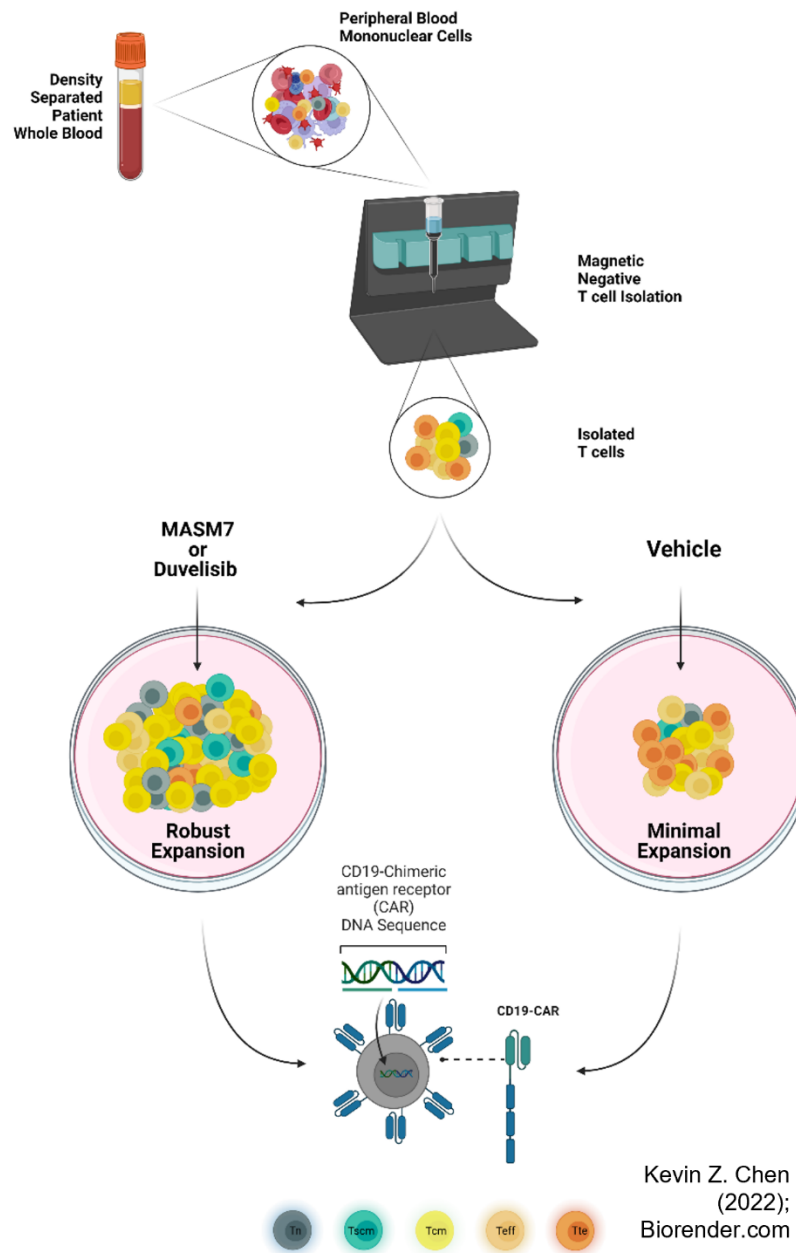


Figure 5. Experimental workflow for *in vitro* studies. First, peripheral blood mononuclear cells (PBMCs) are isolated from CLL patient whole blood or healthy donor aphaeresis samples. Isolated PBMCs are then aliquoted in an appropriate cell freezing medium and stored in gas phase liquid nitrogen for subsequent experiments. Prior to T cell culture and expansion, we isolate “untouched” bulk T cells by negative immunogenic isolation using a Magnetic Activated Cell Sorter (MACS) apparatus. Isolated T cells are stimulated and expanded in culture medium supplemented with Duvelisib, MASM7, or vehicle. T cells from each treatment group are then subjected to flow cytometry, fluorescent and electron imaging, metabolic flux, and western blot assays to determine whether enhancement of mitochondrial fusion improves Tn, Tscm, and Tcm expansion and persistence. This experimental workflow will serve as the basic backbone to my thesis. Furthermore, a significant increase in the number and prevalence of Tn, Tscm, or Tcm subsets in duvelisib or MASM7 groups will suggest that the T cell expansion strategies I have proposed herein can effectively improve upon existing CART manufacturing strategies.

Research Summary

The overarching aim of this thesis is to evaluate the essential role of mitochondrial fusogens, MFN1/2, in the expansion of therapeutically relevant T cell subsets, including T_n, T_{scm}, and T_{cm}. As part of the studies described herein, I interrogated the hypothesis that enhancement of MFN1/2 activity, using a PI3K δ/γ inhibitor (duvelisib) or a mitofusin activating small molecule (MASM7), augments T cell expansion and persistence *ex vivo* such that direct activators of MFN1/2 can improve the efficacy of adoptive T cell therapies for the treatment of hematological malignancies (Figure 5).

I found that increased MFN1/2 protein expression in bulk T cells treated *ex vivo* with duvelisib correlated with increased mitochondrial membrane potential to mass ratios and increased spare respiratory capacity in CD8⁺ T cells. Additionally, duvelisib promotes the expression of proteins involved in anti-apoptotic, epigenetic, and mitophagy pathways that converge on MFN1/2, including sirtuins 1 and 3, PINK/PARKIN, and anti-apoptotic proteins. Of these affected pathways, the SIRT1/3-MFN1/2 axis serves as a potential cross section between PI3K signaling cascades, mitochondrial fusion, and epigenetic reprogramming (**Figure 6**). Interestingly, T cell cultures treated with MASM7 doses between 100nM - 250nM daily for nine days have >50% more CD8⁺ and CD8⁺CD27⁺CD45RO⁻ T cells, compared to duvelisib and vehicle control groups. In addition, MASM7 induces significant increases in mitochondrial volume per mitochondrion and mitochondrial membrane potential to mass ratios, indicative of enhanced mitochondrial fusion.

Taken together, the research described herein represents the first study to investigate 1) the role of MFN1/2 in mediating T cell expansion and persistence downstream of PI3K δ/γ inhibition and 2) the use of direct mitofusin agonists in adoptive cellular therapy. Future studies will evaluate the *in vivo* efficacy of MASM7-treated CARTs and examine potential synergism between direct mitofusin agonists (MASM7) and PI3K inhibitors (duvelisib). It is my hope that my thesis research will inform our foundational understanding of

fusogens of the outer mitochondrial membrane and mitochondrial fusion in relation to T cell memory, expansion, and persistence. Furthermore, the long-term goal of my work is to improve the efficacy of adoptive T cell therapies for the treatment of hematological malignancies.

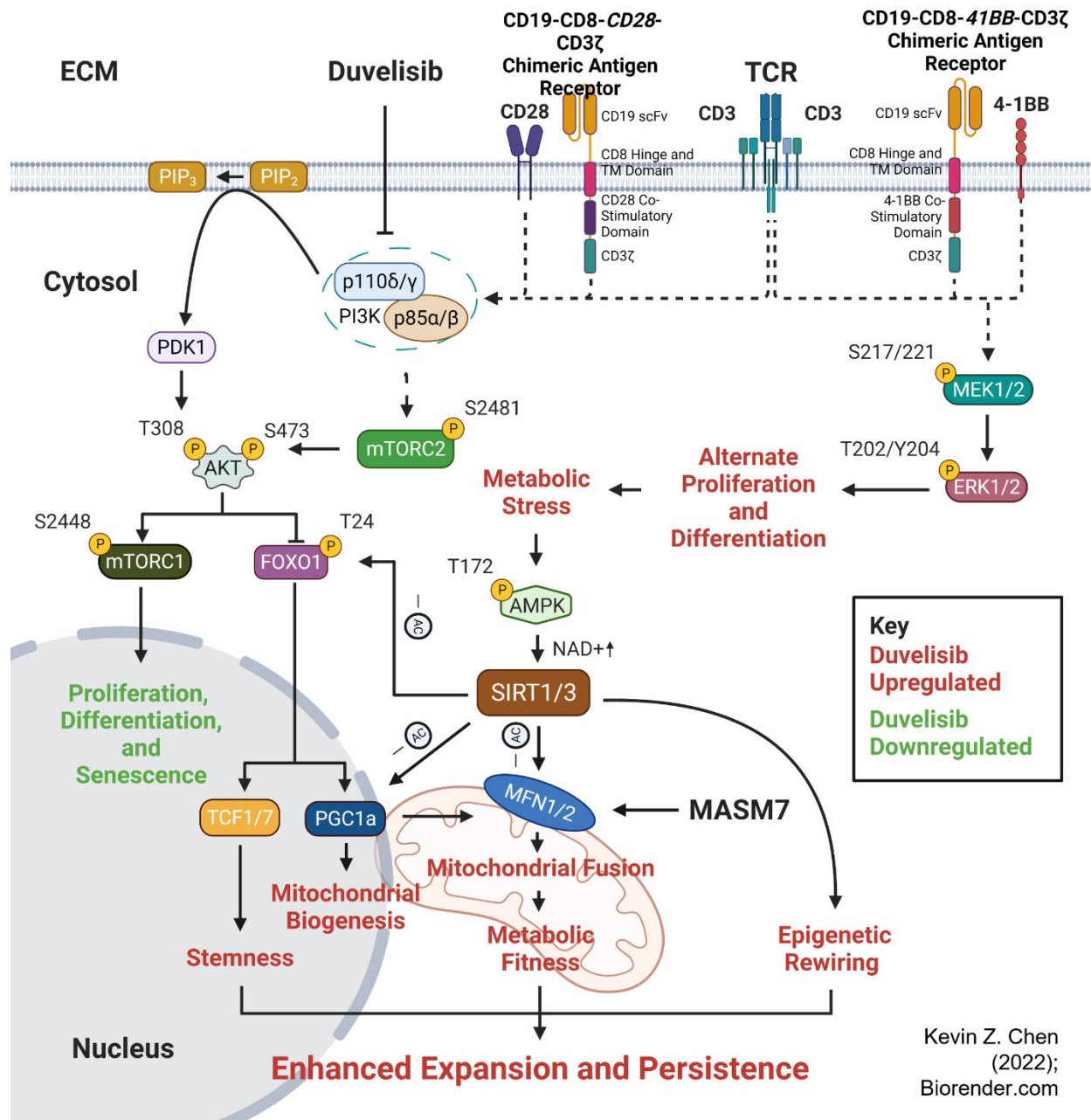


Figure 6. PI3K δ/γ dual inhibition with duvelisib and MFN1/2 activation with MASM7 converge to promote Tn/Tcm expansion and persistence. Duvelisib inhibits PI3K/AKT-driven programs to prevent downstream proliferation, differentiation, and senescence. Inhibition of PI3K signaling cascades induces T cell memory programs, including activation of FOXO1 and TCF1/7 transcription factors. SIRT1 and SIRT3 have been shown to directly activate MFN1/2 through deacetylation²⁻⁶. PINK/PARKIN proteins ubiquitinate MFN1/2 for degradation to initiate mitophagy (not shown). MASM7 induces conformational activation of MFN1/2 to promote tethering of neighboring mitochondria and mitochondrial fusion. I *hypothesize that mitochondrial fusion from active MFN1/2 enhances naïve and central memory T cell expansion and persistence.*

Results

Inhibition of PI3K δ/γ favors mitofusin expression and activity

Because activated Tn (CD45RA+CD45RO-CCR7+) and Tcm (CD45RA-CD45RO+CCR7+) contain more fused and networked mitochondria than Tem (CD45RA-CD45RO+CCR7-) or Temra (CD45RA+CD45RO-CCR7-), I sought to assess the protein expression of known regulators of mitochondrial fusion and fission.^{24, 36}

T cells isolated from Rai Stage 0-2 CLL patient donors were cultured in media containing 300nM duvelisib or a vehicle control of 0.01% DMSO for 14 days following stimulation with anti-CD3/CD28-coated beads and 30IU/mL hIL-2. T cell cultures were re-stimulated on day 9 of culture with anti-CD3/CD28-coated beads per manufacturer's suggestion and $\geq 5 \times 10^6$ cells per treatment group were harvested for immunoblot analysis.¹ Consistent with previous findings that increased mitochondrial fusion promotes Tcm development, I found that T cells treated with duvelisib displayed marked increases in MFN1/2 ($p < 0.05$, $n=5$) and decreases in serine 637 phosphorylation of DRP1 ($p < 0.05$, $n=3$), an indicator of active DRP1 fission activity (**Figure 7**). While not the focus of the research described herein, the effect of PI3K δ/γ inhibition on the expression and activity of OPA1, an essential GTPase of the mitochondrial fission machinery, will be the focus of future T cell studies.^{26, 37, 38}

Subsequently, I assessed the expression of peroxisome proliferator-activated receptor gamma coactivator 1-alpha (PGC1a; a transcriptional coactivator of mitochondrial biogenesis) and translocase of outer membrane 20 (TOM20; often assessed as a surrogate for quantifying mitochondrial mass). In its lesser known role, PGC1a induces MFN1/2 transcription.³⁹⁻⁴¹ While I expected mitochondrial biogenesis and mass to be elevated in T cells with abundantly fusing mitochondria, immunoblot analysis revealed no significant increases in expression of TOM20 (ns , $n=5$), nor PGC1a (ns , $n=3$) (**Figure 7**). Since PGC1a expression is negatively regulated by AKT phosphorylation of FOXO1 at Thr24, I speculate that duvelisib

promotes sustained PGC1a activity and MFN1/2 activation in T cells.^{39, 40} Interestingly, there were coincident increases in expression of cytosolic sirtuin-1 (SIRT1, $p < 0.05$, $n = 6$) and mitochondrial sirtuin-3 (SIRT3, $p < 0.05$, $n = 3$) (**Figure 7**). SIRT1 can deacetylate both MFNs and SIRT3 can deacetylate MFN2 to promote mitofusin stability in human and murine hepatocytes and cardiomyocytes.^{2, 4, 5, 42} While it is unclear whether similar regulatory mechanisms affect MFN1/2 in T cells, MFN1/2 stabilization by SIRT1/3 in other cell types suggests a potential mechanism for MFN1/2 accumulation and increased mitochondrial fusion downstream of PI3K δ/γ inhibition. In addition, my findings that MFN1/2 expression increases in the absence of PI3K δ/γ kinase activity reflects work from the Ghosh group suggesting that active PI3K signaling cascades initiate MFN2 degradation in activated human T cells.⁴³ Therefore, our protein expression analysis suggests that MFN1/2 expression increases in T cells following duvelisib co-culture, and sustained expression of PGC1a and increased SIRT1/3 expression indicate potential mechanisms for amplification of MFN1/2 activity.

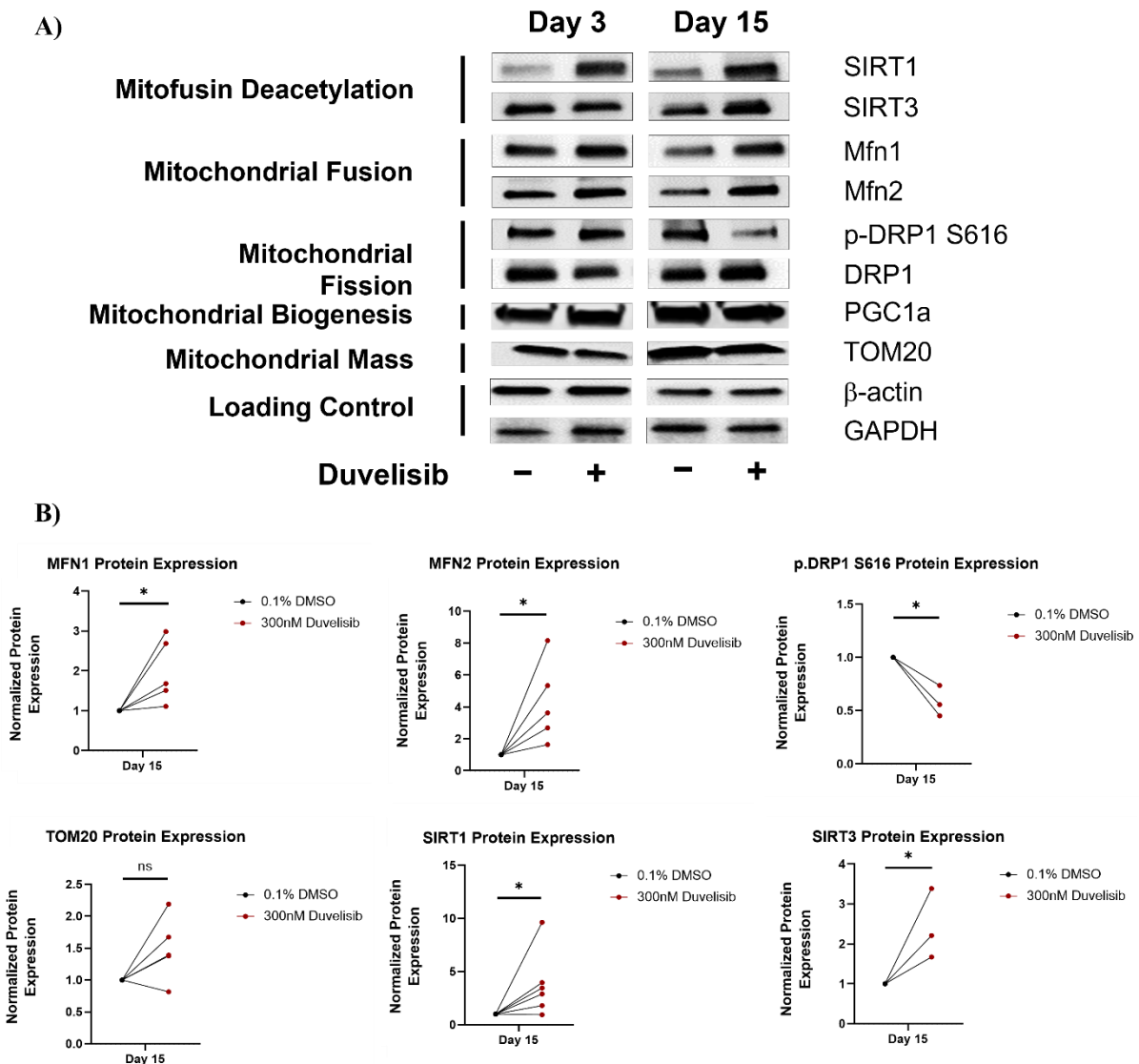


Figure 7. Regulators of mitochondrial dynamics are differentially affected by inhibition of PI3K δ/γ . T cells were harvested on days 3 and 15 of culture following stimulation and co-culture with duvelisib or vehicle. T cells were re-stimulated with α CD3/CD28 coated beads on day 9 on culture. Protein lysates were prepared from harvested T cells using commercially available RIPA buffer supplemented with protease and phosphatase inhibitors. Lysates for T cell harvested on days 3 and 15 were loaded and imaged on the same immunoblot. A) Representative immunoblot images depict protein expression with or without duvelisib treatment on day 3 or 15 of culture. Immunoblots are grouped by the indicated proteins' known role in mitochondrial morphology and dynamics. B) Quantification of protein expression normalized to that of vehicle (0.1% DMSO). Immunoblot band intensities were calculated using FIJI software to determine relative protein expression. Relative expression of key proteins was normalized to that of loading controls corresponding to each biological replicate. Biological replicates correspond to T cells from unique CLL patient samples ($p < 0.05$, $n \geq 3$).

Transmission electron microscopy imaging suggests inhibition of PI3K δ/γ favors fusion

To validate that increases in MFN1/2 expression corresponded to active mitochondrial fusion that produced functional mitochondrial networks, non-transduced T cells and CD19-CAR transduced T cells from CLL patient donors were cultured in media containing 300nM duvelisib or a vehicle control of 0.01% DMSO for 14 days following stimulation with anti-CD3/CD28 antibody coated beads and 30IU/mL hIL-2.¹ On day 15 of culture, $\sim 3 \times 10^6$ cells per treatment group were harvested for mitochondrial imaging by transmission electron microscopy (TEM).

Fixed T cell samples were processed and sectioned for imaging on a JEOL JEM-1400 Standard/Cryo TEM in collaboration with the Integrated Electron Microscopy Core at Emory University. Total mitochondrial cross-sectional area relative to total cell area was manually quantified in collaboration with Dr. Ronnie Funk using FIJI (ImageJ) software rendering of ten or more T cells in resulting TEM images. Mitochondrial cross-sectional area relative to total cell area was not significantly greater in duvelisib-treated T cells (duv-T) (ns, n=4; **Figure 8a**). However, mitochondria of duv-CART had a 1.5-fold increase in mitochondrial cross-sectional area relative to total T cell cross-sectional area compared to control CART (p=0.0013, n=2; **Figure 8b**). The discrepancy in TEM imaging results between untransduced T cells and transduced CART could be due to uneven sample sectioning during the grid preparation process and bias during the imaging process, where sample grids reflected sections of cells regardless of their spatial orientation during fixation and only cells with visible nuclei and mitochondria within each grid were selected for imaging. Because mitochondria are known to cluster near the site of TCR stimulation, it is plausible that our imaging technique was not reflective of the total mitochondrial content within each cell, nor were we able to capture the extent of mitochondrial networking within each cell.^{44,45} Although these data support my earlier findings that duvelisib increases MFN1/2 expression and suggests a correlation between PI3K δ/γ inhibition and mitochondrial fusion, our two-dimensional imaging technique using TEM did not sufficiently capture

mitochondrial networking and dynamics in our T cell model. Thus, for the remainder of the studies described herein, I have used a three-dimensional fluorescent widefield imaging technique on a super-resolution DeltaVision OMX Structured Illumination Microscopy (SIM) microscope.

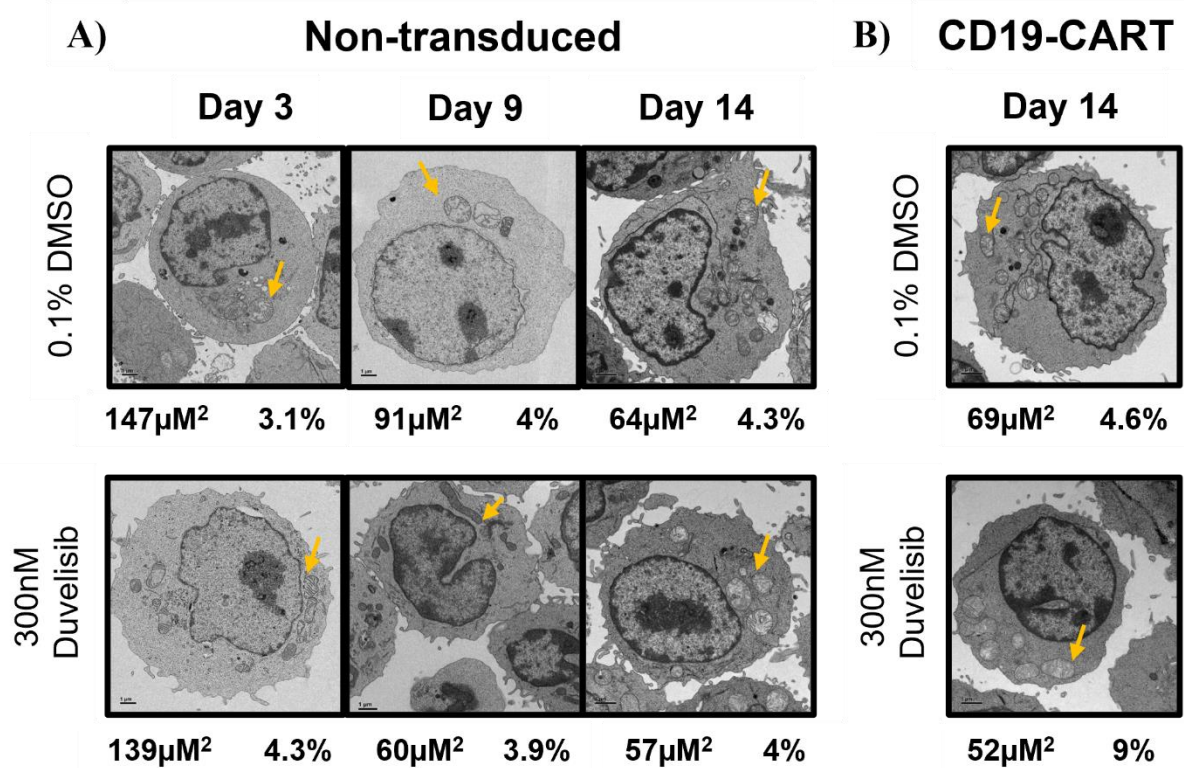


Figure 8. TEM images suggests that duvelisib does not increase mitochondrial fusion. Non-transduced and CAR transduced T-cells were grown for 14 days and analyzed by TEM. Representative TEM images depict two dimensional mitochondrial sections (yellow arrow) in single T cells centered in the grid of view. Labels below each image denote the average mitochondrial cross-sectional area for each treatment condition (bottom left) and average mitochondrial cross-sectional area as a percentage of total cell area (bottom right). In collaboration with Dr. Funk at Emory University, FIJI software was used measure T-cell size across >10 replicate images for each patient sample and treatment condition in non-transduced (n=5) and CART (n=2) T cell studies.

Differences in mitochondrial quality between patients may predict response to duvelisib

To further examine the relationship between PI3K δ/γ inhibition, MFN1/2 upregulation, and mitochondrial fusion, I investigated changes to mitochondrial respiratory capacity and membrane potential in duv-T, both correlate measures of mitochondrial fusion.

To evaluate the respiratory capacity of MFN1/2 overexpressing T cells, I designed a series of metabolic flux experiments using the Seahorse instrument. On day 15 of co-culture with duvelisib or vehicle, I harvested replicate wells of growing CLL patient-derived T cells, a portion of which were sorted into CD4+ or CD8+ T cell subsets by column-free immunomagnetic negative separation. Subsequently, bulk CD3+ and sorted CD4+ or CD8+ T cells were re-plated onto Seahorse assay-specific cell cartridges and subjected to a mitochondrial stress test pre-programmed on the Agilent Seahorse XFe24 instrument available to me through the Winship Cancer Institute at Emory University. The mitochondrial stress test consists of a series of twelve metabolic flux measurements acquired over the course of two hours during which pharmacological modulators of respiration (oligomycin, carbonyl cyanide-4 (trifluoromethoxy) phenylhydrazone (FCCP), and rotenone/antimycin A) are administered to assess T cell metabolic responses during respiratory stress. The output measures include oxygen consumption rate (OCR; proportional to rate of cellular respiration), extracellular acidification rate (ECAR; proportional to rate of glycolysis), and spare respiratory capacity (SRC; difference between maximal and basal respiration; predictive of the capacity of cells to respond to increased energy demand).¹

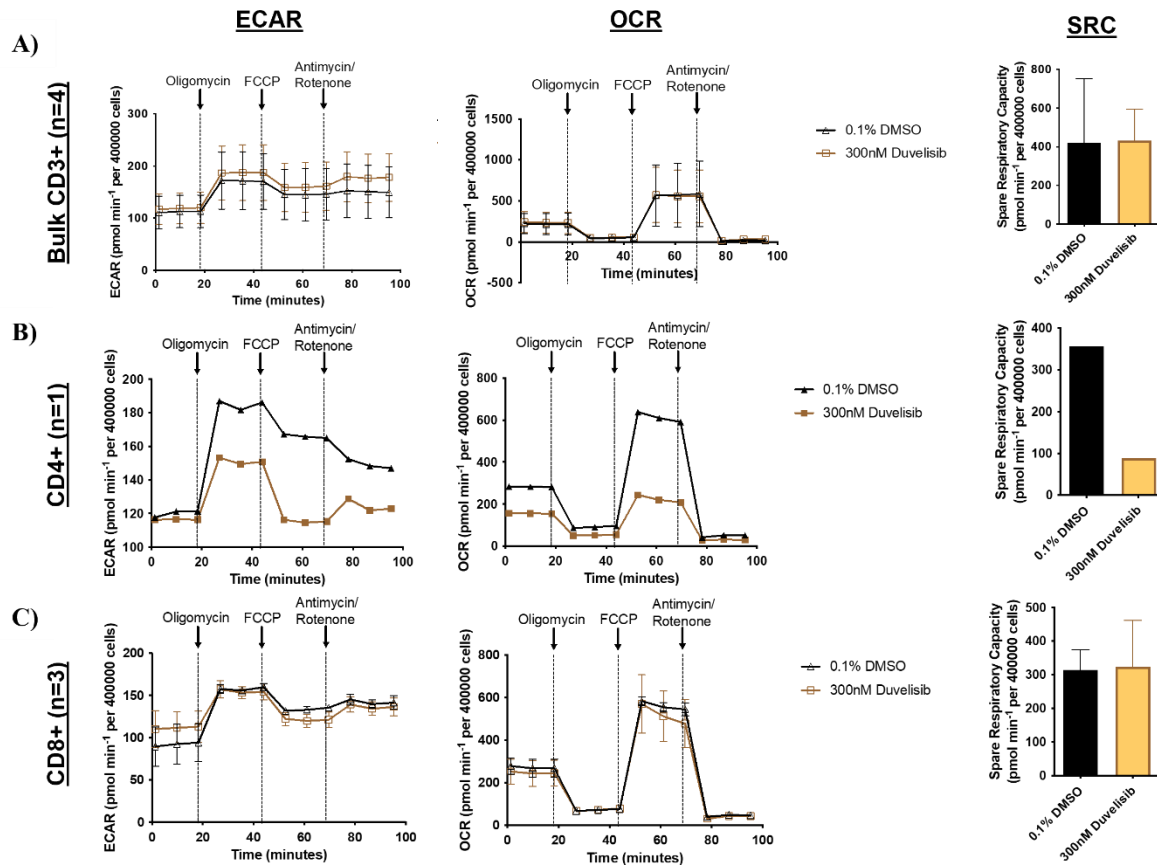


Figure 9. Duvelisib does not increase respiratory capacity of untreated CLL patient T cells. OCR, ECAR, and SRC measurements from untreated Rai Stage 0-1 CLL donors were plotted using GraphPad Prism software. ECAR, OCR, and SRC plots (columns) depict measurements acquired on a Seahorse XFe24 Metabolic Flux Analyzer for A) bulk CD3⁺ (ns, n=4), B) CD4⁺ (n=1), and C) CD8⁺ (ns, n=3) T cells following 15 days of co-culture with duvelisib (gold) and vehicle (black). Measures are normalized to the cell number of 400,000 T cells per well. Number of biological replicates was restricted by cell number and viability following cell harvest and sorting such that only samples with $\geq 2.5 \times 10^6$ cells were subjected to metabolic flux analysis.

Unexpectedly, metabolic flux analysis of bulk CD3⁺ T cells did not reveal significant differences in OCR, ECAR, and SRC between duvelisib or vehicle groups (**Figure 9A**). In addition, of the three unique CLL patient-derived T cell cultures sorted into CD4⁺ and CD8⁺ T cell subsets, only one sample yielded sufficient CD4⁺ T cells following cell sorting for metabolic flux analysis (data not shown). Therefore, while duvelisib appeared to lower the OCR, ECAR, and SRC in CD4⁺ T cells, the limited sample size hindered

my ability to assess the significance of this finding (**Figure 9B**). Interestingly, CD8+ T cells isolated from the same set of T cell cultures presented no appreciable differences in OCR, ECAR, or SRC compared to control (**Figure 9C**). Although T cells from the sorting experiments were expanded in parallel from untreated CLL patient samples with Rai Stage 0 or 1 disease, I could not discount the possibility that heterogeneity in patient and disease characteristics could confound the results of my experiments. Therefore, I repeated the Seahorse metabolic flux experiments using T cells expanded from healthy and ibrutinib pre-treated CLL patient samples (**Figure 10**).

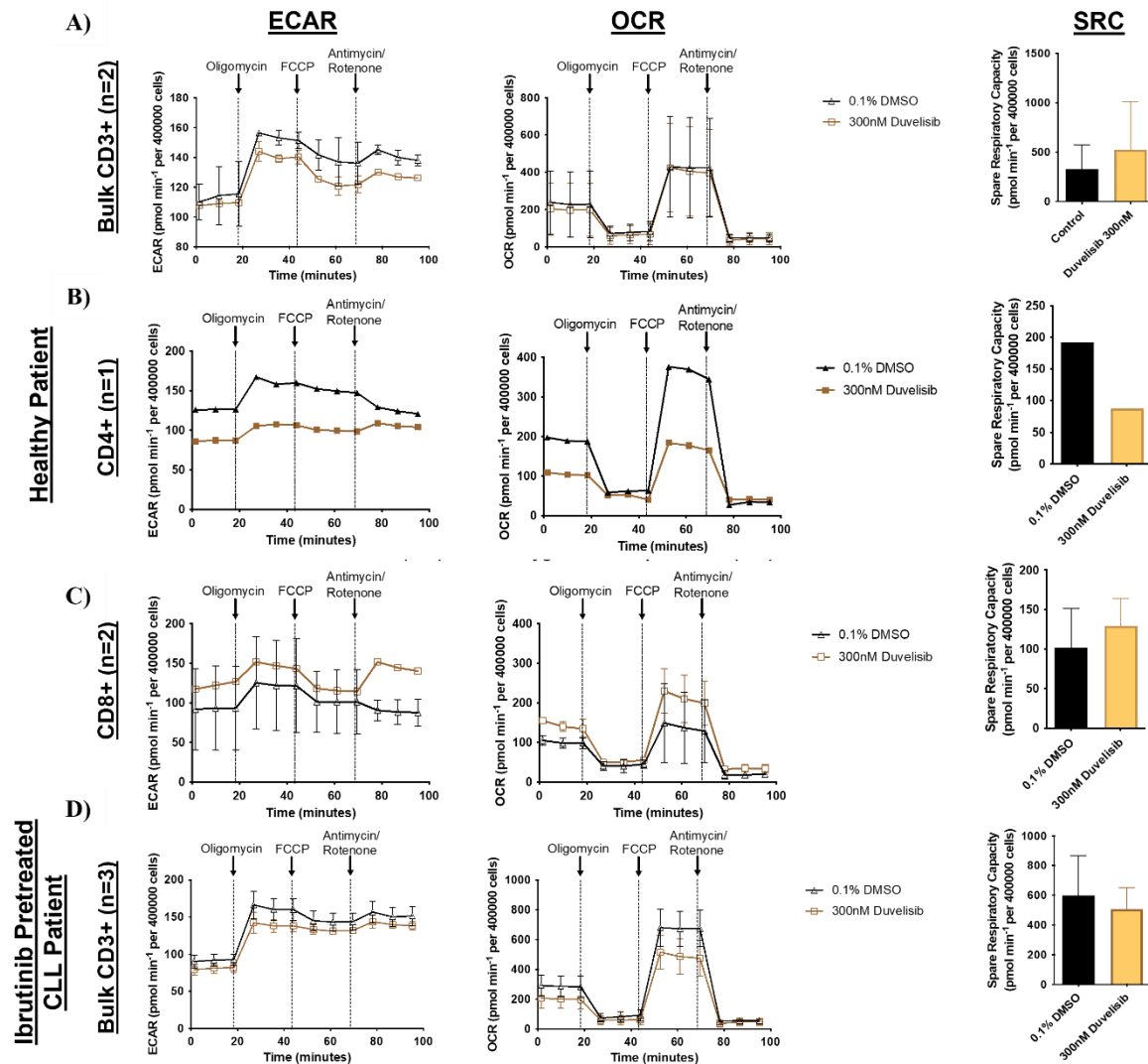


Figure 10. Duvelisib favors respiration and glycolytic compensation in healthy donor T cells. OCR, ECAR, and SRC measurements were plotted using GraphPad Prism software. ECAR, OCR, and SRC plots (columns) depict measurements acquired on a Seahorse XFe24 Metabolic Flux Analyzer for healthy donor A) bulk CD3+ (ns, n=2), B) CD4+ (n=1), and C) CD8+ (ns, n=2) T cells following 15 days of co-culture with duvelisib (gold) and vehicle (black). ECAR, OCR, and SRC plots for bulk CD3+ T cells from ibritinib pre-treated CLL patient samples are depicted in D). Measures are normalized to the cell number of 400,000 T cells per well. Number of biological replicates was restricted by cell number and viability following cell harvest and sorting such that only samples with $\geq 2.5 \times 10^6$ cells were subjected to metabolic flux analysis.

As with T cells expanded from untreated CLL patient samples, the ECAR, OCR, and SRC of bulk CD3+ T cells from healthy donor samples does not significantly change with duvelisib (**Figure 10A**). However,

the observed decrease in ECAR, OCR, and SRC in the duvelisib group is more pronounced in CD4+ healthy donor-derived T cells (**Figure 10B**). In addition, duvelisib appreciably decreases the glycolytic rate and respiratory capacity of ibrutinib pre-treated CLL patient T cells more than untreated CLL patient T cells compared to respective controls (**Figure 10D**).

The final drug-treatment of cells during the Mito Stress Test is a combination of ETC inhibitors consisting of rotenone (complex I inhibitor) and antimycin A (complex III inhibitor) that shuts down mitochondrial respiration and enables the calculation of non-mitochondrial respiration driven by processes outside the mitochondria, such as glycolysis. Of note, CD8+ healthy donor T cells from the duvelisib group have appreciably higher OCR and SRC (**Figure 10C**). Preliminarily, CD8+ duv-T from healthy donors appear to upregulate glycolysis following respiratory collapse, as seen in the tail-end spike in ECAR following rotenone and antimycin A administration, a phenomenon not seen in control counterparts.

Mitochondrial depolarization refers to the dissipation of the mitochondrial inner membrane potential ($\Delta\psi_m$), driven by ion gradients required for mitochondrial ATP synthesis. When $\Delta\psi_m$ drops below a certain threshold, mitochondrial damage-induced autophagy (mitophagy) programs are triggered, resulting in the preferential degradation of impaired mitochondria.^{46, 47} Therefore, changes to $\Delta\psi_m$ correlate to the accumulation of mitochondrial damage such that low $\Delta\psi_m$ is indicative of high mitochondrial damage. As $\Delta\psi_m$ and MFN1/2-mediated mitochondrial fusion are interdependent, I hypothesized that high mitofusin expression following PI3K δ/γ inhibition enhances mitochondrial membrane polarity and low $\Delta\psi_m$.⁴⁸⁻⁵⁰

Following 15 days of co-culture with duvelisib or vehicle, I assessed changes to mitochondrial membrane potential and mass using fluorescent MitoTracker Green FM (MitoTracker Green) and Deep Red FM (MitoTracker Deep Red) dyes. While both MitoTracker Green and Deep Red dyes stain mitochondria in live cells, retention of MitoTracker Deep Red in mitochondria is $\Delta\psi_m$ dependent, such that MitoTracker

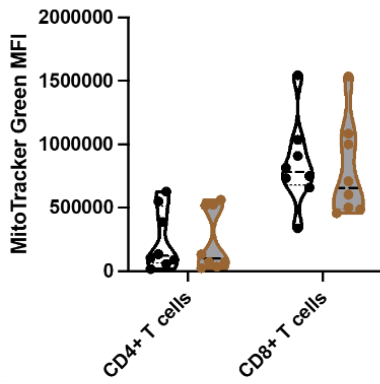
Deep Red staining decreases with decreasing $\Delta\psi_m$.⁵¹ Because MitoTracker Green stains mitochondria irrespective of $\Delta\psi_m$, evaluating differences in MitoTracker Green and Deep Red staining by flow cytometry and the ratio of MitoTracker Green to Deep Red mean fluorescent intensity (MFI) provides a robust system for interrogating mitochondrial membrane potential in *duv*-T.⁵²

Previous studies have demonstrated that CD4⁺ T cells have higher basal glycolysis while CD8⁺ T cells rely heavily on OXPHOS for cytokine production.⁵³ Consistent with these findings, mitochondrial mass and membrane potential are generally higher in CD8⁺ T cells than CD4⁺ T cells in both treatment groups (**Figure 11A-B**). When comparing CD4⁺ T cells from paired samples harvested on days 3 and 15, changes in mitochondrial mass and membrane potential correlate to the sample which the T cells originated irrespective of duvelisib treatment, suggesting that inherent differences between the two CLL patient samples dictated whether mitochondrial mass and membrane potential would increase or decrease following prolonged T cell culture (**Figure 11C-D**). However, I did not observe this result in CD8⁺ T cells, elucidating that the degree of glycolytic dependency within CD4⁺ populations prior to T cell expansion may predict mitochondrial function in CD4⁺ T cells following prolonged culture (**Figure 11E-F**). Finally, duvelisib improves the mitochondrial membrane potential to mass ratio in a portion of patient T cell samples for both CD4⁺ and CD8⁺ T cell subsets (**Figure 11G**).

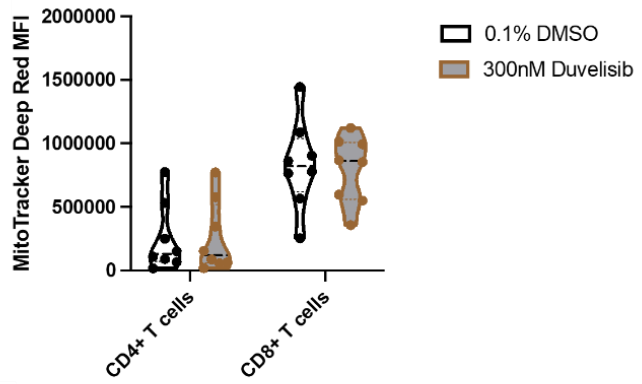
Mitochondrial Mass

Mitochondrial Membrane Potential

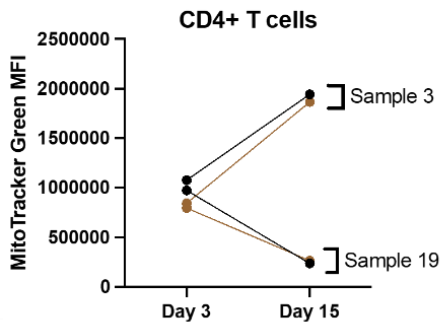
A)



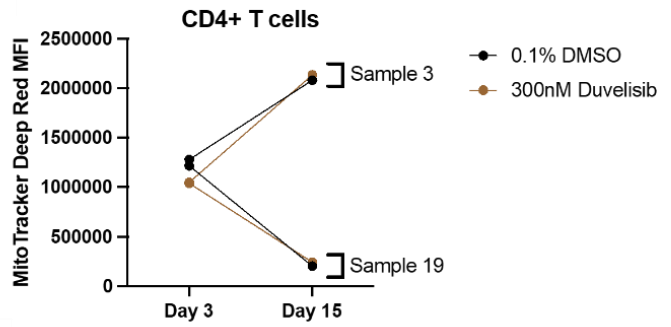
B)



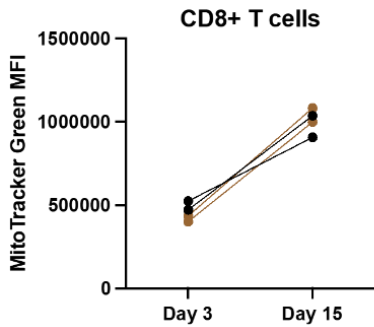
C)



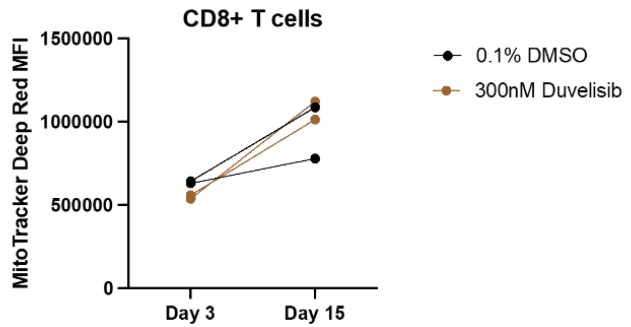
D)



E)



F)



G)

**Mitochondrial Membrane Potential to Mass Ratio
Day 15 of T cell Expansion**

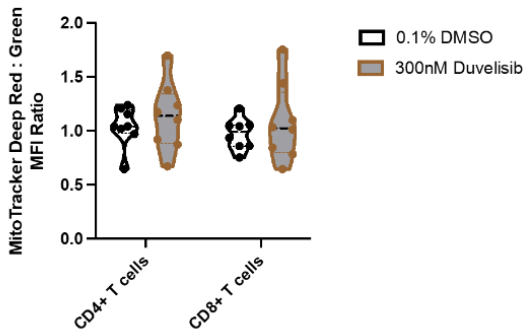


Figure 11. Mitochondrial mass and membrane potential of CD4+ T cells change following prolonged T cell culture irrespective of duvelisib treatment. T cells harvested on Days 3 and 15 of culture were immunolabeled with antibodies against surface antigens at room ambient temperature prior to staining with MitoTracker dyes at 37°C for 20 minutes followed by flow cytometry data acquisition. Panels depict plots of MitoTracker Green MFI values (left column) and MitoTracker Deep Red MFI values (right column). Violin plots the first row compare A) mitochondrial mass and B) membrane potential of CD4+ and CD8+ T cells expanded in the presence of duvelisib (gold) or vehicle (black). Panels C-F compare C) mitochondrial mass of CD4+ T cells, D) mitochondrial membrane potential of CD4+ T cells, E) mitochondrial mass of CD8+ T cells, and F) mitochondrial membrane potential of CD8+ T cells harvested on days 3 and 15 of expansion with or without duvelisib. Panel G compares the mitochondrial membrane potential to mass ratio computed as the MFI of MitoTracker Deep Red:MFI of MitoTracker Green in CD4+ (Panel G left) and CD8+ (Panel G right) T cells.

Taken together, the metabolic flux and flow cytometry data suggest that the relationship between duvelisib-mediated MFN1/2 overexpression and expansion of Tn, Tscm, and Tcm subsets does not entirely depend upon the ability of MFN1/2 to promote mitochondrial fusion and OXPHOS metabolism. I hypothesize that the sum of all mitofusin activities within duv-T cultures (e.g., mitochondrial fusion, mitophagy, mitochondrial trafficking, mitochondrial outer membrane permeabilization (MOMP), and calcium ion (Ca²⁺) flux through crosstalk with the endoplasmic reticulum) supports the expansion and persistence of Tn, Tscm, and Tcm subsets downstream of PI3K δ/γ inhibition.

Duvelisib induced pathways converge on MFN1/2

To investigate the involvement of mitophagy, cell survival, and epigenetic pathways downstream of PI3K δ/γ inhibition in the expansion and persistence of Tn, Tscm, and Tcm subsets, I assessed the expression of proteins involved in each of the aforementioned pathways by immunoblot.

As with my earlier immunoblot experiments, T cells isolated from Rai Stage 0-2 CLL patient donors were cultured in media containing 300nM duvelisib or a vehicle control of 0.01% DMSO for 14 days following stimulation with anti-CD3/CD28-coated beads and 30IU/mL hIL-2. T cell cultures were re-stimulated on

day 9 of culture with anti-CD3/CD28-coated beads and $\geq 5 \times 10^6$ cells per treatment group were harvested for immunoblot analysis.

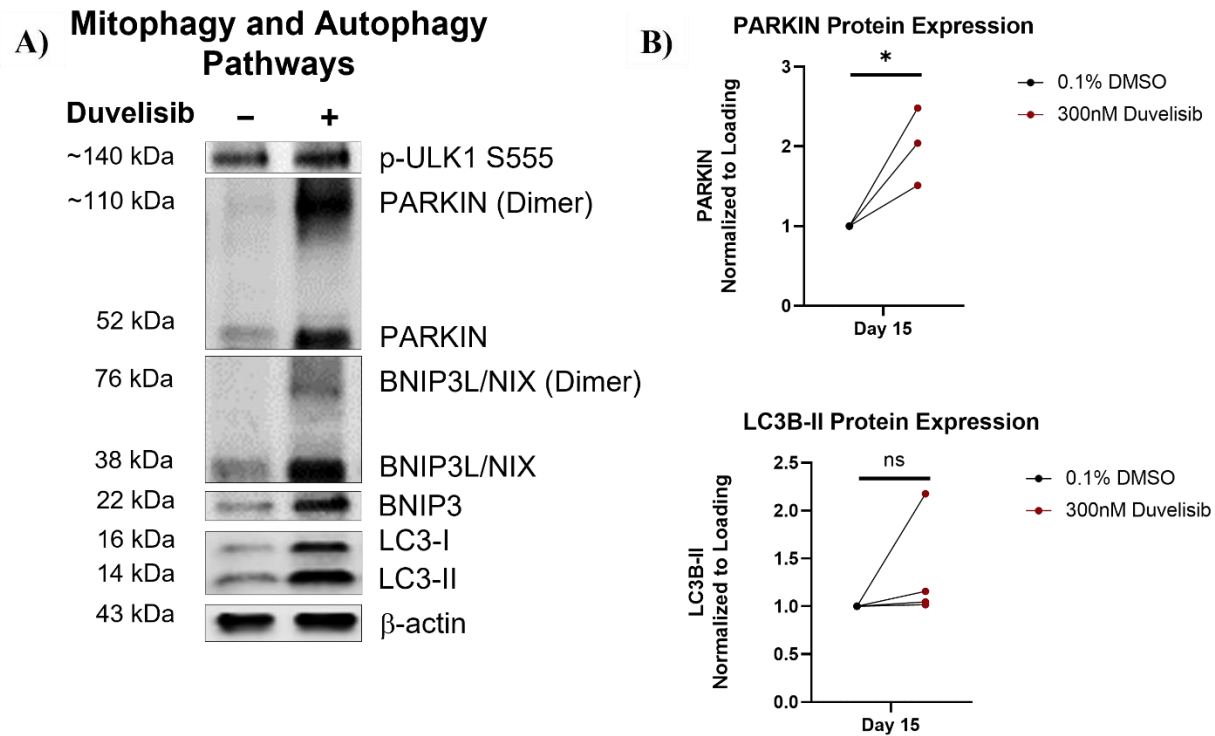


Figure 12. Mitophagy pathways are upregulated in duv-T. T cells were harvested on day 15 of culture following stimulation and co-culture with duvelisib or vehicle. Protein lysates were prepared from harvested T cells using commercially available RIPA buffer supplemented with protease and phosphatase inhibitors. A) Representative immunoblot images depict expression of mitophagy-related proteins with or without duvelisib treatment on day 15 of culture. B) Quantification of protein expression normalized to vehicle. Immunoblot band intensities were calculated using FIJI software to determine relative protein expression. Relative expression of key proteins was normalized to that of loading controls corresponding to each biological replicate. Biological replicates correspond to T cells from unique CLL patient samples. * $p < 0.05$; ns=not significant.

Proteins involved in mitophagy and autophagosome formation, including Parkin, an E3-ubiquitin ligase, ($p < 0.05$, $n = 3$) and phosphatidylethanolamine-conjugated autophagy marker Light Chain 3 (LC3), are highly expressed in duv-T cells (**Figure 12A**). Mechanistically, mitochondrial depolarization triggers PINK1, a serine/threonine kinase, to activate and recruit Parkin to the mitochondrial outer membrane. Parkin ubiquitinates OMM proteins, including MFN1/2, as one of the first steps of the PINK1/Parkin

mitophagy pathway.⁵⁴ During autophagosome biogenesis, LC3-I is converted to LC3-II by lipidation, LC3-II is incorporated into the membrane of autophagosomes, and later on in the mitophagy process, is degraded by lysosomal proteases.⁵⁵ While high LC3-II expression and significant increases in Parkin expression could suggest active mitophagy in *duv*-T cells, additional studies investigating dynamic LC3-II turnover are required (**Figure 12B**). Additionally, high expression of Bcl-2/adenovirus E1B interacting protein 3 (BNIP3) and BNIP3-ligand (NIX)

further support the hypothesis that mitophagy is activated in duvelisib-treated T cells (**Figure 12A**). Meanwhile, as a pro-apoptotic BH3-only protein, BNIP3 is known to induce DRP1-mediated mitochondrial fission, interact with Bcl-2 family proteins (e.g. Bcl-2/Bcl-xL), and activate effectors of apoptosis (e.g. Bak/Bax).^{56,57} Although increases in the expression of anti-apoptotic proteins (Bcl-2, Mcl-1 long, and Bcl-xL) and corresponding decreases in cleaved caspase-3 suggest that duvelisib may promote T cell survival programs, I also observed concurrent high expression of BCL2-interacting mediator of cell death (Bim) and related apoptotic protein (Bid) (**Figure 13**). Future studies employing co-immunoprecipitation techniques will assess protein complexes formed between these pro- and anti-apoptotic proteins. Due to the similar size of anti-apoptotic proteins probed in this panel between 30-50kda, I attempted to use vinculin (124 kDa)

Anti- and Pro-Apoptotic Pathways

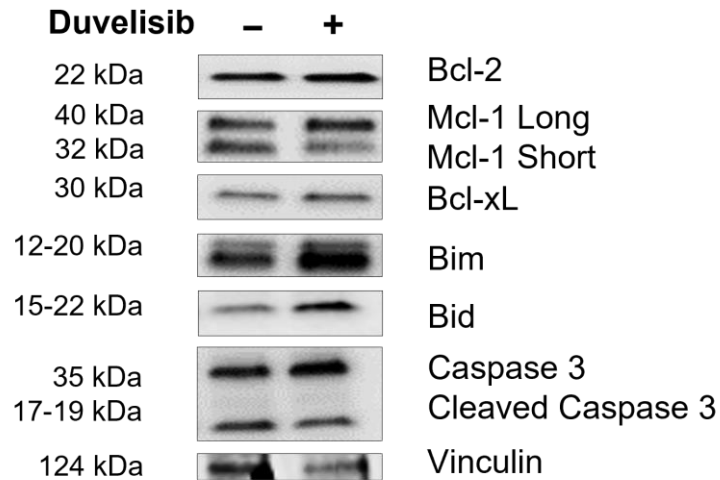


Figure 13. Duvelisib induces expression of both apoptotic and anti-apoptotic proteins. T cells were harvested on day 15 of culture following stimulation and co-culture with duvelisib or vehicle. Protein lysates were prepared from harvested T cells using commercially available RIPA buffer supplemented with protease and phosphatase inhibitors. Representative immunoblot images depict expression of cell death-related proteins with or without duvelisib treatment on day 15 of culture. No quantification was conducted due to poor quality of loading control blots.

as an alternative loading control with limited success. Thus, further experimentation is required to determine the significance of these findings (**Figure 13**).

On the other hand, duvelisib enhances histone 3 lysine 27 trimethylation ($p < 0.05$, $n = 4$), an epigenetic mark associated with the repression of CD4⁺ T cell differentiation and promotes memory programs in CD8⁺ T cells (**Figure 14**). Furthermore, duv-T significantly overexpressed proteins associated with the maintenance of T cell memory programs (EZH2, FOXO1, FOXO3, ID3, and TCF1/7) without similar increases in DNMT3a, a DNA-methyltransferase critical in directing T cell differentiation into effector T cells (**Figure 14**). In addition to SIRT1 and SIRT3, expression of mitochondrial deacylase, SIRT5 is enhanced in duv-T

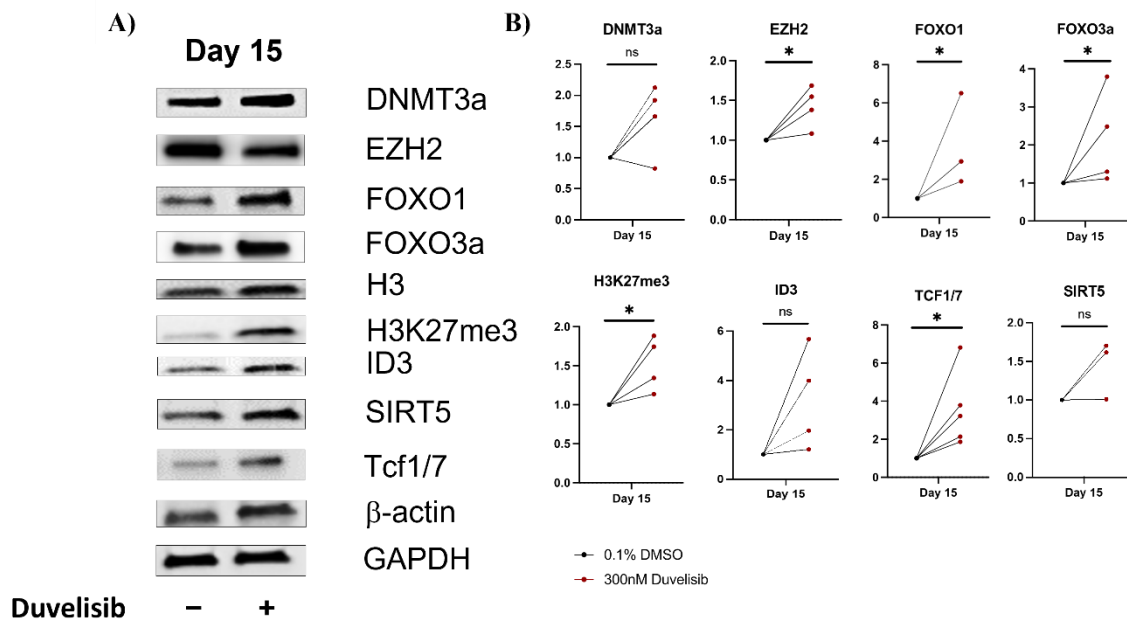


Figure 14. Duvelisib favors memory T cell programs. T cells were harvested on day 15 of culture following stimulation and co-culture with duvelisib or vehicle. Protein lysates were prepared from harvested T cells using commercially available RIPA buffer supplemented with protease and phosphatase inhibitors. A) Representative immunoblot images depict expression of proteins with or without duvelisib treatment on day 15 of culture. B) Quantification of protein expression normalized to vehicle, including DNMT3a (ns, $n = 3$), EZH2 ($p < 0.05$, $n = 3$), FOXO1 ($p < 0.05$, $n = 3$), FOXO3a ($p < 0.05$, $n = 4$), H3K27me3 ($p < 0.05$, $n = 3$), ID3 (ns, $n = 4$), TCF1/7 ($p < 0.05$, $n = 5$), and SIRT5 (ns, $n = 3$). Immunoblot band intensities were calculated using FIJI software to determine relative protein expression. Relative expression of key proteins was normalized to that of loading controls corresponding to each biological replicate. Biological replicates correspond to T cells from unique CLL patient samples. * $p < 0.05$; ns=not significant.

(**Figure 14**). To interrogate my previous findings that the sirtuin-mitofusin axis serves a potential bridge between epigenetic regulation and mitochondrial fusion, I activated healthy donor-derived T cells with anti-CD3/CD28 beads, re-stimulated T cells on day 9 of culture, and harvested $\geq 3 \times 10^6$ T cells daily over the course of the 15-day expansion for immunoblot analysis. In the absence of duvelisib, expression of SIRT1 with an activating phosphorylation at serine 47 (phospho-S47-SIRT1) strongly correlated with MFN1 and MFN2 expression, including concurrent recovery of phospho-S47-SIRT1, MFN1, and MFN2 between day 11 to day 15 of T cell expansion following re-stimulation (**Figure 15**). However, expression of the catalytically inactive and truncated form of SIRT1 decreased steadily over the course of T cell expansion (**Figure 15**).

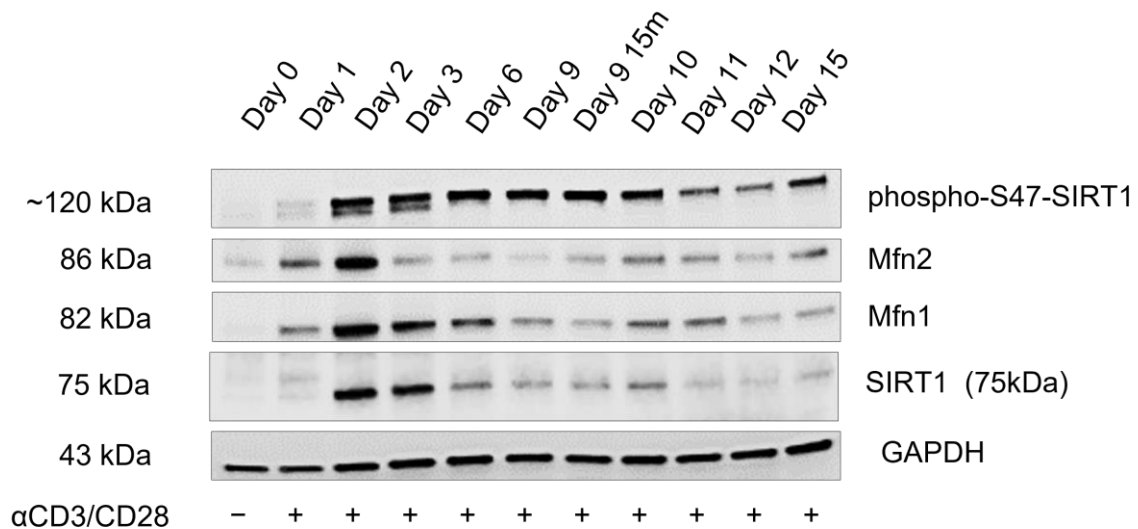


Figure 15. SIRT1 activity and MFN1/2 coincide during prolonged *in vitro* T cell culture. T cells were harvested daily between days 0 to 15 of culture following activation on day 0 with α CD3/CD28 beads. “Day 9 15m” denotes T cell lysates collected from cultures 15 minutes after re-stimulation with α CD3/CD28 beads, while “Day 9” lysates were collected before re-stimulation. All protein lysates were prepared from harvested T cells using commercially available RIPA buffer supplemented with protease and phosphatase inhibitors. Protein concentration was normalized for protein loading using a Bradford assay prior to SDS-PAGE. Representative immunoblot images depict protein expression of catalytically active and inactive forms of SIRT1 as well as MFN1/2. No quantification was conducted.

These data inform my theory that SIRT1 serves as a potential enhancer of MFN1/2 stability, such that MFN1/2 accumulation and activity facilitate pathways required for the maintenance and persistence of memory T cells, including mitophagy, cell survival, and epigenetic reprogramming. Moreover, variability in T cell expansion, mitochondrial morphology, and metabolism between untreated CLL, ibrutinib pre-treated CLL, and untreated donors highlight that treatment status and disease stage are important considerations in predicting expansion failure during *ex vivo* co-culture with duvelisib, where use of direct activators of MFN1/2 serve as alternatives to modulating T cell metabolism through PI3K inhibitors (**Figure S1**).

MASM7 promotes CD8+ T cell expansion and mitochondrial fusion

To evaluate MASM7 as a suitable T cell expansion reagent, CLL patient T cells were activated with soluble anti-CD3/CD28 antibodies and expanded in the presence of 30 IU/mL IL-2 and 62.5nM-500nM MASM7, 300nM duvelisib, or vehicle. For this set of experiments, I shortened the length of T cell culture to 8 days to improve the clinical relevance of my expansion protocol. On day 8, T cells were harvested and evaluated for T cell phenotype and three-dimensional (3D) mitochondrial morphology by flow cytometry and widefield microscopy. Soluble anti-CD3/CD28 antibodies were used in place of beads for these experiments to facilitate downstream imaging experiments. For flow cytometry experiments, T cell populations were gated on viable cells using the FlowJo analysis platform such that T cells with compromised permeabilized membranes were excluded from analysis.

Paired comparisons of T cell cultures from individual donors indicate that MASM7 consistently improves T cell expansion (**Figure 16A**). Due to stark differences in the number of viable T cells between cultures from different CLL donors, differences in numbers of expanded T cells do not appear significant when analyzed across multiple donors. To account for the fold differences in viable cell number between donor T cell samples, I first calculated the fold-expansion of each T cell culture (dividend of day 8 and day 0

numbers of viable cells). The fold-expansion and frequencies of T cell subsets on day 8 were then normalized to that of the respective vehicle group.

CLL patient-derived T cells treated with 125nM of MASM7 expanded >50% more than vehicle ($p < 0.05$, $n = 3$) and >100% more than duvelisib counterparts ($p < 0.05$, $n = 3$) (**Figure 16B**). Treatment with 125nM MASM7 significantly enhanced the expansion of CD8 and CD27 co-expressing T cells (CD8+CD27+) ($p < 0.05$, $n = 3$) and decreased the frequency of TIM-3 and LAG-3 co-expressing CD8+ T cells ($p < 0.05$, $n = 3$), suggesting that T cells expanded from MASM7-treated cultures have clinically significant phenotypes (**Figure 16C-D**). Higher or lower doses of MASM7 (62.5nM, 250nM, and 500nM) resulted in non-significant trends towards increased T cell expansion, consistent with an optimal effect at 125nM MASM7. Future experiments evaluating Carboxyfluorescein succinimidyl ester (CFSE) staining and Ki-67 immunolabeling of resultant T cells will improve our understanding of cellular proliferation following MASM7 treatment.

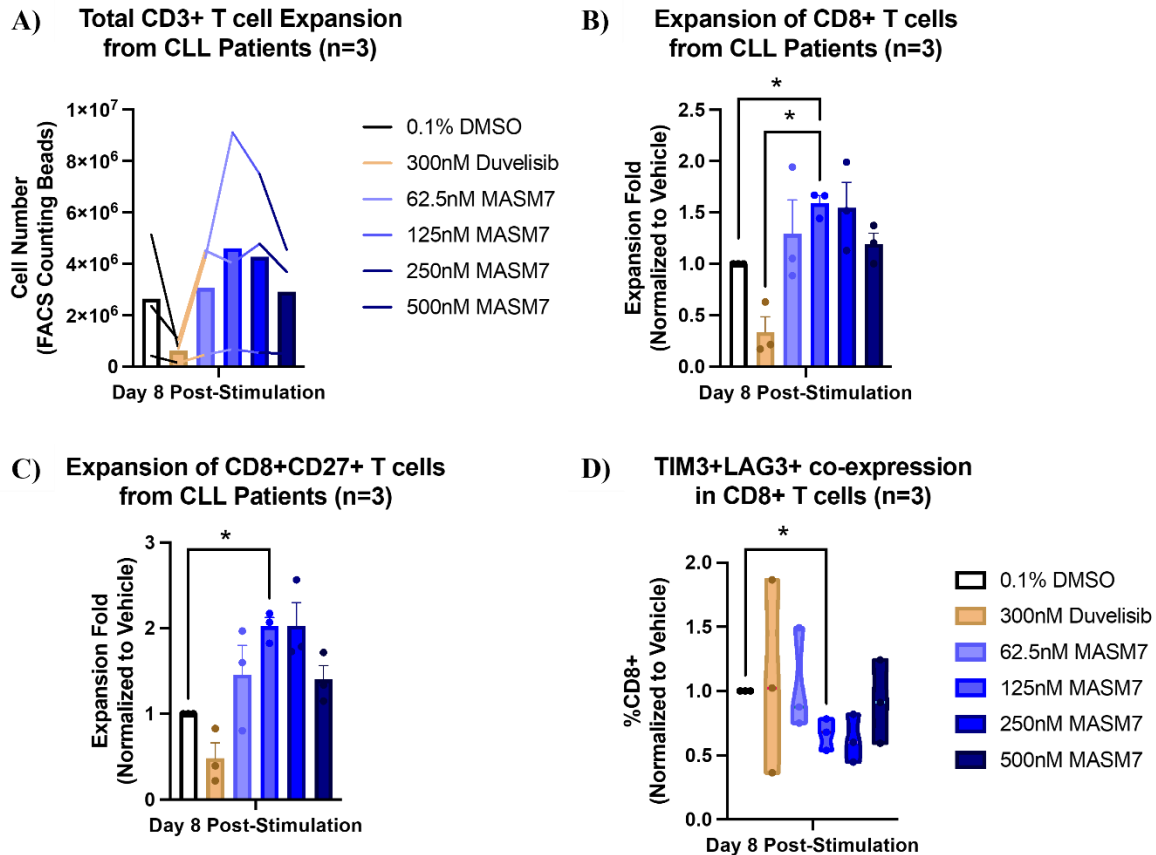


Figure 16. MASM7 augments T cell expansion. T cells from CLL donors were activated with soluble α CD3/CD28 activator, cultured with 0.1% DMSO (vehicle), 300nM duvelisib, or various doses of MASM7, and immunolabeled for surface marker expression on day 8 of culture. T cell data was acquired on a 5-laser Cytex Aurora spectral cytometer prior to analysis on FlowJo software. Commercial counting beads were used during flow acquisition to calculate cell number. Plots depict A) total number of CD3+ T cells expanded from 200,000 plated cells over the course of 8 days, B) relative expansion of CD8+ T cells, C) relative expansion of CD8+CD27+ T cells, and D) relative frequency of TIM3+LAG3+ co-expressing cells within the CD8+ compartment. Relative expansion fold and frequency denotes normalization to vehicle. * $p < 0.05$; ns=not significant.

To assess whether observed T cell phenotypes can be attributed to the specific activity of MASM7 on MFN1/2 and mitochondrial fusion, I compared differences in mitochondrial morphology between T cells cultured in the presence of 62.5-500nM MAMS7, 300nM duvelisib, or vehicle. On day 8 of culture, T cells were harvested and immunolabeled for CD4, CD8, and mitochondrial import receptor subunit (TOM20;

protein ubiquitously expressed by mitochondria). Using a DeltaVision OMX Super-Resolution SIM microscope, I acquired stacks of widefield microscopy images taken sequentially along the z-plane, each of which depict a single cell. Then, I reconstructed z-stacked images of the same cell into 3D projections, which were masked for quantification of mitochondrial volume in voxels (μm^3).

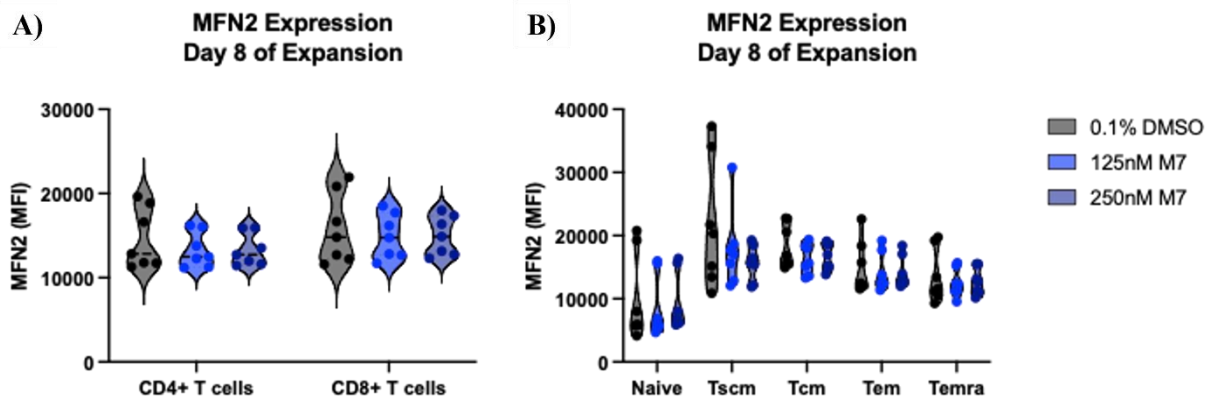


Figure 17. MASM7 does not affect MFN2 expression. T cells from CLL donors were activated with soluble $\alpha\text{CD3}/\text{CD28}$ activator, cultured with 0.1% DMSO (vehicle), 300nM duvelisib, or various doses of MASM7, and immunolabeled for surface marker and intracellular MFN2 expression on day 8 of culture. T cell data was acquired on a 5-laser Cytex Aurora spectral cytometer prior to analysis on FlowJo software. Commercial counting beads were used during flow acquisition to calculate cell number. Plots depict A) MFN2 expression plots as mean MFI in CD4+ and CD8+ T cells from vehicle treated cultures and B) MFN2 expression plots as mean MFI in CD8+ T cell subsets, including Tn, Tscm, Tcm, Tem, and Temra. * $p < 0.05$; ns=not significant.

Direct comparison of MFN2 expression between CD4+ and CD8+ T cells reveals that MFN2 expression varies significantly between patient samples following expansion (**Figure 17A**). While Tscm and Tcm subsets express the highest levels of MFN2, MASM7 treatment at the effective doses of 125nM and 250nM do not affect MFN2 expression level compared to control (**Figure 17B**). Furthermore, only addition of MASM7 to T cell cultures significantly augmented the mitochondrial volume of individual mitochondrion ($p < 0.05$, $n \geq 212$ mitochondria from ≥ 10 CD8+ T cells from one donor), suggesting that MASM7, but not duvelisib, promotes mitochondrial fusion in CLL patient T cells (**Figure 18A-B**). Coincidentally, the mitochondrial membrane potential to mass ratio is higher in CD8+ T cells treated with MASM7 compared

to duvelisib and vehicle (**Figure 18C**), further supporting the specific activity of MASM7 on MFN1/2 activity and mitochondrial fusion. Future studies utilizing a MFN1/2 genetic knockout T cell model will improve our understanding of the MFN1/2-specific effects of MASM7. In addition, doses between 125nM and 250nM of MASM7 should be interrogated to identify the optimal dose of MASM7 conducive to mitochondrial fusion and therapeutic T cell expansion.

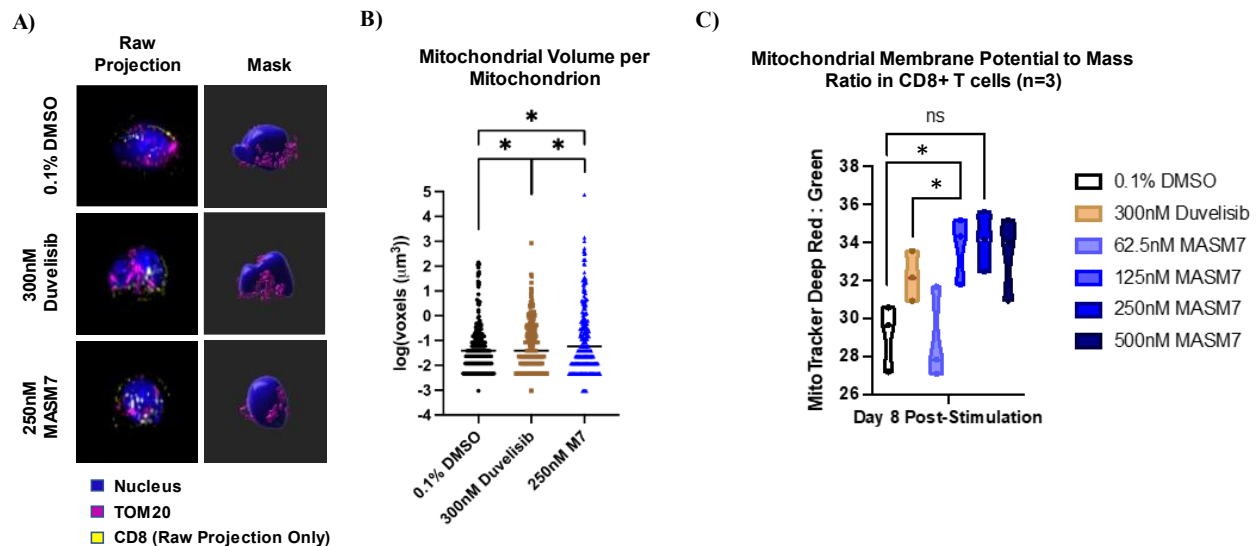


Figure 18. MASM7 augments T cell expansion. T cells from CLL donors were activated with soluble anti-CD3/CD28 activator and cultured with 0.1% DMSO (vehicle), 300nM duvelisib, or various doses of MASM7. On day 8 of culture, T cells were harvested, fixed in 4% paraformaldehyde, and stained for surface CD4 (not shown), CD8 (yellow), mitochondrial TOM20 (violet), and nuclear DNA (blue). Z-stacks of single-cell, widefield images acquired on a DeltaVision OMX SIM microscope were reconstructed as 3D projections in A) (left). Nuclei and mitochondria fluorescent signals, but not CD8, were masked to mark distinct organelle borders A) (right). B) Mitochondrial volume per individual/networked mitochondria was quantified using Imaris software and graphed in GraphPad Prism. C) Mitochondrial membrane potential to mass ratio was evaluated by flow cytometry and plotted in GraphPad Prism as discussed in **Figure 11**. * $p < 0.05$; ns=not significant.

Discussion

During my investigation of duvelisib as an inducer of MFN1/2 protein expression, I found that the ability of duvelisib to promote T_n, T_{scm}, and T_{cm} expansion, persistence, and function may not be related to MFN1/2-mediated mitochondrial fusion. Instead, upregulation of MFN1/2-related mitophagy, cell survival, and epigenetic pathways may serve as effector pathways that promote T cell memory programs downstream of PI3K δ/γ inhibition (**Figures 6, 12-14**). Moreover, the SIRT1-MFN1/2 axis may serve as an intersection between PI3K δ/γ inhibition and MFN1/2 activity (**Figures 7, 15**). Future research will investigate whether sorted individual CD8⁺ T cell subsets have differences in mitochondrial fusion and metabolism despite the non-significant differences in mitochondrial membrane potential and respiratory capacity of CD8⁺ T cells overall. Additionally, Seahorse metabolic flux analysis and flow cytometry phenotyping of duv-CART harvested from OSU-CLL engrafted recipient mice may elucidate the prolonged effect of duvelisib on the metabolic characteristics of therapeutic T cells *in vivo*.

Several clinical trials registered on the clinical trial database (clinicaltrials.gov) of the National Institutes of Health have sought to investigate the efficacy of duvelisib as an oral monotherapy for the treatment of relapsed and refractory CLL/Small Lymphocytic Lymphoma and Non-Hodgkin Lymphoma (NHL).⁵⁸ While the completed Phase III DUO (NCT02004522) and Phase II Dynamo (NCT01882803) studies suggest that duvelisib may have clinically meaningful activity in heavily pre-treated CLL/SLL and NHL patients, the U.S. Food and Drug Administration withdrew approval of the relapsed or refractory follicular lymphoma indication for duvelisib (COPIKTRA) in 2021 due to the manufacturer's (SecuraBio, Inc.) inability to conduct a clinical trial to verify clinical benefit of duvelisib in follicular lymphoma.⁵⁹ Despite the wavering efficacy of duvelisib *in vivo*, pre-clinical studies from our laboratory, including those described in this thesis, Funk et al. (*Blood*, 2021), and the recruiting DEEP-T CELLS clinical trial (NCT04890236), may suggest a role for duvelisib as a therapeutic T cell expansion reagent.^{1, 60}

On the other hand, MASM7 augments the expansion of CD8+ T cells, including Tn and Tcm subset, with coincident increases in mitochondrial fusion and membrane potential, presumably through its function as a direct MFN1/2 activator (**Figures 16-17**). As a first-in-class small molecule activator of previously “undruggable” mitofusin proteins, the capacity of MASM7 to expand therapeutically relevant T cell subsets provides a promising avenue in the realm of mitochondrial targeting during the expansion of T cells for adoptive cellular therapies. Still, significant characterization and optimization remains to elucidate the advantages and limitations of MASM7 as a T cell expansion reagent.

In conclusion, improving our mechanistic understanding of mitochondrial dynamics T cells elucidates novel methods of metabolic targeting for the improvement of cancer immunotherapy, where PI3K δ/γ inhibitors and direct mitofusin agonists may synergize or serve as effective single agents for the expansion of therapeutic T cells with the overarching goal of improving cancer immunotherapy and cancer patient outcomes.

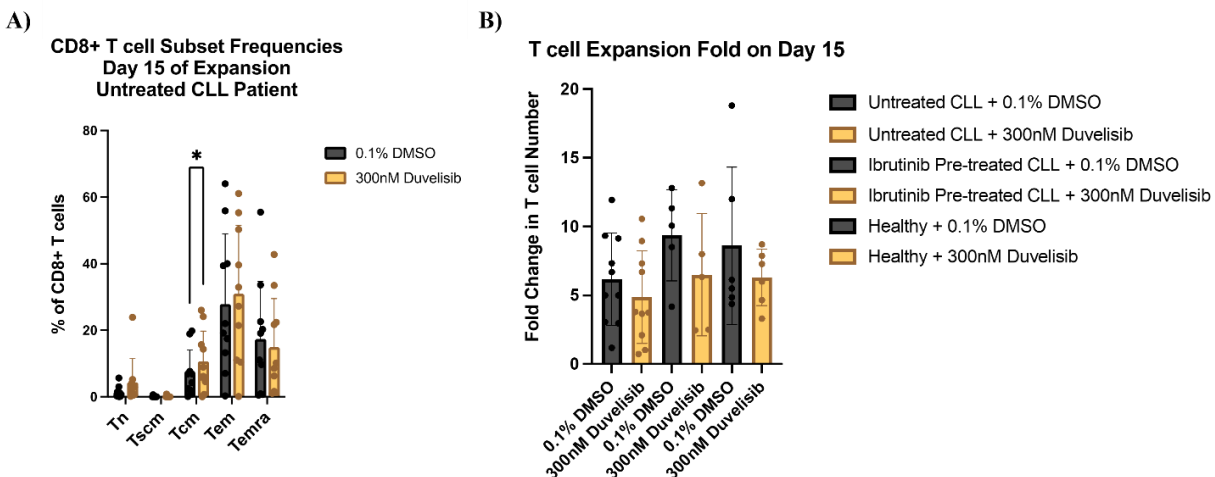


Figure S1. Duvelisib expands Tcm as well as pre-treated CLL and healthy donor T cells. T cells from CLL donors were activated with anti-CD3/CD28 beads and cultured with 0.1% DMSO (vehicle), or 300nM duvelisib. On day 9 of culture, T cells were re-stimulated with anti-CD3/CD28 beads. On day 15, T cells were harvested for immunolabeling prior to data acquisition. T cell data was acquired on a 5-laser Cytex Aurora spectral cytometer prior to analysis on FlowJo software. Commercial counting beads were used during flow acquisition to calculate cell number. Bar charts depict A) frequencies of CD8+ T cell subsets expressed as % of CD8+ T cells representing each subset and B) T cell expansion fold derived from total T cell number from each sample for untreated CLL, Ibrutinib pre-treated CLL, and healthy donor T cell samples. * $p < 0.05$; ns=not significant.

Future Directions

To predict patient response to duvelisib or MASM7:

- What biomarkers of CLL patient samples predicts response to duvelisib or MASM7 treatment?
- Does pre-treatment (e.g. ibrutinib) pre-select or synergize with duvelisib or MASM7 treatment?
- Are divergent responses between patient sampled due to differences in drug uptake?

To dissect duvelisib's effect on CD4+ T cells:

- How does duvelisib affect the phenotype of CD4+ T cells (Th1, Th2, Th17, Treg)?
 - Does duvelisib affect memory programs in CD4+ T cells?

To distinguish expansion from enrichment:

- Do duvelisib or MASM7 truly promote the expansion of T cells, or is the observed expansion a result of enrichment for specific T cell clones?
- Does proliferation of various T cell subsets change with duvelisib or MASM7 treatment?
- Does duvelisib or MASM7 affect the resiliency of T cells to apoptosis?

To assess T cell metabolism:

- Does duvelisib or MASM7 alter the metabolic dependency of T cells?
- How does nutrient deprivation (e.g. glucose “starvation”) affect T cells treated with duvelisib or MASM7?
- What is the mitochondrial morphology of duv-CART or MASM7-CART *in vivo*?
- Do MASM7-CART sustain mitochondrial fusion *in vivo*?
- What are the differences in metabolic flux of CD4+ and CD8+ T cell subsets?
- What are the differences in cristae morphology between duv-, MASM7-, and control-CART and how do these morphological differences reflect mitochondrial function?

To assess synergy between MASM7 and duvelisib:

- Do lower doses of duvelisib synergize with MASM7 to promote T cell enrichment, expansion, persistence, or function?

Concluding Remarks

With the closing of my thesis document, I offer my most sincere gratitude to my advisor, Dr. Waller, my thesis committee members, Drs. Henry and Kahn, and my mentors and colleagues at Emory University and beyond for their expertise, brilliant insight, and support during these past few years. To Dr. Gavathiotis, thank you for giving me the distinct privilege of working with this exciting new compound, MASM7. Finally, to MASM7, I hope our paths cross again.

Sincerely,

Kevin Z. Chen

Materials and Methods

Compounds

Duvelisib (IPI-145) was purchased from MedChemExpress (Monmouth Junction, NJ) and stored as a 20mM stock solution in DMSO at -80°C. MASM7 was obtained from the Gavathiotis group at Albert Einstein College of Medicine (Material Transfer Agreement No. A-00005121) and used immediately or stored as a 10mM stock solution in DMSO at -80°C. Dilutions of all compounds were done in DMSO prior to addition to cell cultures, all with a final DMSO concentration of less than 0.1% in all wells.

Complete Media for Human T cell Cultures

For all T cell cultures, RPMI 1640 with L-Glutamine (Lonza; Basel, Switzerland) was supplemented with 10% Fetal Bovine Serum (FBS), 100 U/mL penicillin, 100 µg/mL streptomycin, 50 µM 2-mercaptoethanol, 1mM sodium pyruvate, and 1mM non-essential amino acids.

Table S1. Table of Human Samples

Sample ID	Disease and Stage	Treatment
3	CLL Rai 0	untreated
13	CLL Rai 2	untreated
18	CLL Rai 0	untreated
19	CLL Rai 1	untreated
20	CLL Rai 1	untreated
24	CLL Rai 0	untreated
27	CLL Rai 0	untreated
44	CLL Rai 0	untreated
68	CLL Rai 2	untreated
113	CLL Rai 0	untreated
116	CLL Rai 0	untreated
185	CLL Rai 0	untreated
190	CLL Rai 0	untreated
198	CLL Rai 0	untreated
221	CLL Rai 1	untreated
225	CLL Rai 0	untreated
235	CLL Rai 0	untreated
279	CLL Rai 0	untreated
300	CLL Rai 0	untreated
333	CLL Rai 0	untreated
419	CLL Rai 0	untreated
427	CLL Rai 0	untreated
507	CLL Rai 0	untreated
515	CLL Rai 0	untreated
535	CLL Rai 1	untreated
558	CLL Rai 0	untreated
843	CLL Rai 2	untreated
885	CLL Rai 0	untreated
2499	CLL Rai 0	untreated
Ibru85	CLL	on ibrutinib
Ibru215	CLL	on ibrutinib
Ibru178	CLL	on ibrutinib
Ibru22	CLL	on ibrutinib
Ibru562	CLL	on ibrutinib
Ibru174	CLL	on ibrutinib
Ibru509	CLL	on ibrutinib
HD898	Healthy	Not applicable
HD928	Healthy	Not applicable
HD405	Healthy	Not applicable
HD119	Healthy	Not applicable
HD874	Healthy	Not applicable
HD118	Healthy	Not applicable

Table S2. Table of Flow Cytometry Reagents

Marker (Phosphorylation)	Fluorochrome	Catalog Number	Manufacturer	Dilution (1 x 10 ⁶ Cells/100uL buffer)
Annexin V	PE-CF594	563544	BD	1:50
CCR7	BV711	353228	BioLegend	1:50
CCR7	BV785	353230	BioLegend	1:50
CCR7	Pacific Blue	353210	BioLegend	1:50
CD2	PE-Cy5	555328	BD	1:25
CD27	BV650	302828	BioLegend	1:50
CD27	BV711	302834	BioLegend	1:50
CD28	APC	559770	BD	1:25
CD28	BV605	562976	BD	1:50
CD3	PE-CF594	562280	BD	1:50
CD3	PE-Cy5	300410	BioLegend	1:50
CD4	APC-Cy7	557871	BD	1:50
CD45RA	PE-Cy7	25-0458-42	Invitrogen	1:50
CD45RO	BB700	745807	BD	1:50
CD8	AF700	557945	BD	1:50
CD8	Pacific Blue	558207	BD	1:50
CD95 (Fas)	BV785	305646	BD	1:50
Ki-67	BV605	350522	BD	1:25
KLRG1	FITC	130-120-425	Miltenyi Biotec	1:50
LAG3	PE	565616	BD	1:50
LIVE/DEAD Fixable Aqua	Live Dead Aqua	L34966	ThermoFisher	1:1000
LIVE/DEAD Fixable Yellow	Live Dead Yellow	L34959	ThermoFisher	1:1000
MFN2	CL594	CL594-67487	ProteinTech	1:50
MitoTracker Deep Red FM	AF647	M22426	Invitrogen	50nM
MitoTracker Green FM	MTG	M7514	Invitrogen	50nM
PD-1	BV711	564017	BD	1:50
PD-1	PE-CF594	565024	BD	1:50
TCF1/7	PE	14456S	CST	1:50
TCF1/7	AF488	6444S	CST	1:50
TIM3	BV421	565562	BD	1:50
TIM3	BV605	742856	BD	1:50
FcyRII Blocker (CD32)	FcR Block	18520	STEM Cell	1:50
BD Stain Buffer Plus		566385	BD	1:20
Cell Staining Buffer		420201	BioLegend	100uL

Table S3. Table of Western Blot Antibodies

Protein	Phosphorylation	Catalog Number	Manufacturer	Dilution
a-Actinin (Direct HRP Conjugate)		12413S	CST	1:1000
Akt	S473	4060S	CST	1:500
Akt		9272S	CST	1:1000
Akt	T308	13038S	CST	1:1000
B-actin		4970S	CST	1:1000
Bcl-2		3498S	CST	1:1000
Bcl-xL		66020-1-1g	ProteinTech	1:2000
Bid		8762S	CST	1:500
Bim		NBP1-75511	Novus	1:500
Caspase 3		9662S	CST	1:1000
Citrate Synthase		14309S	CST	1:1000
DNMT3A		3598S	CST	1:1000
DRP1	S637	4867S	CST	1:500
DRP1		8570S	CST	1:1000
EZH2		5246S	CST	1:1000
FoxO1		2880T	CST	1:1000
FoxO1/FoxO3	T24/T32	9464T	CST	1:1000
FoxO3a		2497S	CST	1:1000
GAPDH		5174S	CST	1:1000
Histone H3		9715S	CST	1:1000
Histone H3K27Me3		9733S	CST	1:1000
ID2		3431S	CST	1:1000
ID3		9837S	CST	1:1000
LC3B		2775S	CST	1:1000
Mcl-1		94296S	CST	1:1000
Mfn-1		14739S	CST	1:1000
Mfn-2		9482S	CST	1:1000
anti-Ms IgG (HRP)		ab6789	Abcam	1:5000
Ms IgG Isotype Control		5415S	CST	1uL
Parkin (Prk8)		4211S	CST	1:1000
PGC1a		NBP1-04676	Novus	1:1000
PINK1		6946S	CST	1:1000
anti-Rb IgG (HRP)		ab205718	Abcam	1:5000
Rb IgG Isotype Control		2729S	CST	1uL
SIRT1		ab110304	Abcam	1:1000
SIRT1	S47	2314S	CST	1:2000
SIRT3		5490S	CST	1:1000
SIRT5		8782S	CST	1:1000
TCF1/7		2203S	CST	1:1000
TOM20		42406S	CST	1:1000
ULK1	S555	5869S	CST	1:500
ULK1		8054S	CST	1:1000

Sample Collection, Leukapheresis, and PBMC isolation

This study involving humans was conducted in accordance with the Declaration of Helsinki. De-identified CLL patient samples were collected in collaboration with Dr. Jean Koff and her team of clinicians and clinical research coordinators at Emory Winship Cancer Institute under the Emory IRB-approved protocol for the “Myeloma/Lymphoma Sample Repository” study (Winship 2226; addendum 12). Fresh quarter-sized Human Peripheral Blood Leukopaks each containing ~2.5 billion Peripheral Blood Mononuclear Cells (PBMCs) were purchased from STEMCELL Technologies (Vancouver, Canada) and cryopreserved in CryoStor® CS10 Cell Freezing Medium (STEMCELL Technologies). In some instances, leukapheresis was performed on consenting healthy volunteers (IRB00010018), as described in previous studies from the Waller laboratory.¹ PBMCs were isolated from whole blood donations from CLL patients (IRB00057236 and IRB00046063) by Ficoll-Hypaque density-gradient centrifugation and cryopreserved in Cryostore CS10 buffer (STEMCELL Technologies, Vancouver, Canada).¹ All samples described in this thesis are listed in **Table S1**.

T-cell activation and expansion

All T cell cultures were initiated from cells cryopreserved in liquid nitrogen. Frozen cells were thawed and rested at 37°C in media in a 5% CO₂ humidified incubator for six hours in complete RPMI media.¹ T cells were enriched using a CD3 negative selection kit (EasySep, STEMCELL Technologies) prior to trypan blue (0.4%) staining and cell counting on a Countess Cell Counting Chamber (Invitrogen, Carlsbad, California).

For experiments where duvelisib was the only test compound, anti-CD3/CD28 antibody-conjugated bead stimulation was performed (ThermoFisher-Dynabeads, Waltham, MA) at a 1:1 bead:cell ratio. 30 IU/mL recombinant human IL-2 (R&D systems, Minneapolis, MN) and either duvelisib (MedChemExpress, Monmouth Junction, NJ) or DMSO (VWR, Radnor, PA) was added every three days as previously

described.¹ Cells were cultured in 24 well G-Rex plates with 2 cm² of gas-permeable area (Wilson Wolf, Saint Paul, Minnesota) and re-stimulated with 1:1 cell to bead ratio on day 9 with anti-CD3/CD28 beads. The final DMSO concentration was $\leq 0.1\%$. Aside from TEM experiments, for which the presence of metal beads could affect TEM instruments, anti-CD3/CD28 beads were not removed from T cell cultures prior to experimentation.

In subsequent experiments utilizing both MASM7 and duvelisib, T cells were stimulated with soluble anti-CD3 and anti-CD28 antibodies (ImmunoCult, STEMCELL Technologies). 30 IU/mL recombinant human IL-2 (R&D systems) and either duvelisib (MedChemExpress) or DMSO (VWR) was added every three days, while MASM7 (see *Compounds*) was added daily to accommodate the suspected short half-life of the compound.³⁵

CART experiments

CART experiments described in this thesis were conducted by Drs. Christopher (Ronnie) Funk and Shuhua Wang as described.¹ In brief, CD19-CART were generated via lentiviral transduction of enriched T cells from CLL patients with a CD19-targeting CAR lentiviral construct containing intracellular domains of CD28 and CD3 ζ . Transduced cells were isolated for positive GFP and CD19-CAR expression prior to anti-CD3/CD28 bead stimulation and prolonged culture as previously described. CART were harvested on day 15 for phenotypic analysis or delivery into OCU-CLL-engrafted recipient NOG mice.¹ Parallel TEM experiments using non-transduced T cells were conducted by Mr. Kevin Z. Chen, the author of this thesis.

Flow Cytometry

Characterization of cell cultures was performed prior to and on day 15 or day 8 of cell culture. Cells were stained with LIVE/DEAD Fixable Aqua viability dye (Invitrogen, Carlsbad, California), washed twice with PBS, and stained for thirty minutes at 4°C with antibodies in **Table S2**. The MitoTracker staining protocol

was adapted from Brad Chazotte (CSHL, 2011) and attached to the end of this section. In brief, T cells were stained with 50nM of each MitoTracker dye for ~20 minutes at 37°C prior to flow cytometry acquisition.⁶¹ Data files were acquired on a 4-laser or 5-laser Cytex Aurora spectral cytometer (Cytex Biosciences, Fremont, CA) and analyzed using the version 10 of the FlowJo software (FlowJo, Ashland, Oregon).

Seahorse Assay

Prior to the day of assay, Agilent Seahorse Sensor cartridges were submerged overnight in Agilent Seahorse XF Calibrant at 37°C in a non-CO₂ incubator. Seahorse assay medium (pH 7.4) was prepared using Agilent Seahorse XF Base Medium supplemented with 1mM pyruvate and 2mM glutamine (Agilent Technologies, Santa Clara, CA).

400,000 cells per well were plated in a Seahorse cell culture plate pre-treated with Corning® Cell-Tak Cell and Tissue Adhesive (Corning, NY) and incubated for one hour in assay medium. OCR was measured using the Mito Stress test protocol following injections of oligomycin (2.5 μM), carbonyl cyanide p-trifluoromethoxyphenyl hydrazone (FCCP; 0.5 μM), and antimycin and rotenone (2μM each) on an Agilent Seahorse XF24 bioenergetics analyzer. Oligomycin is an inhibitor of complex V (ATP synthase) (Agilent Technologies, Santa Clara, CA). FCCP is a protonophore that uncouples ATP synthesis from oxygen consumption. Rotenone inhibits complex I and antimycin A inhibits complex III. SRC is calculated as the difference between maximal and basal respiration. Results were analyzed by the Seahorse Wave Controller Software. OCR data was normalized by live cell counts in each sample at the time of plating.⁶²

Immunoblot/Western Blot

5 million cells were lysed in 50uL of RIPA buffer supplemented with protease and phosphatase inhibitor cocktails (ThermoFisher, Waltham, MA), for 15 minutes on ice and centrifuged at 18000 x g for 15 minutes at 4°C to pellet insoluble material. Protein lysate was removed without disturbing the solid pellet and stored

at -20°C until time of assay. The protein concentration of thawed lysates was determined using Bradford reagent (Bio-Rad, Hercules, CA). ~30 µg of lysate was loaded onto a pre-cast 4-20% acrylamide gradient gel (TGX mini, Bio-Rad) and run at 180 V for ~35 minutes. Proteins were transferred onto PVDF membrane using the Trans-Blot® Turbo Semi-Dry Transfer System (Bio-Rad, Hercules, CA). The membrane was blocked in 1% blocker BSA in tris-buffered saline and tween-20 solution (TBS-T) (ThermoFisher) for 1 hour and then incubated with primary and secondary antibodies listed in **Table S3**. When applicable, membranes were stripped using Restore PLUS Western Blot Stripping Buffer (ThermoFisher, Waltham, MA). Blot images were acquired using a chemiluminescent imager (Azure Biosystems, Dublin, CA) and analyzed on FIJI is Just Image J software (NIH, Bethesda, MD). A detailed Western Blot protocol can be found at the end of this section.

Immunofluorescent Staining for Widefield Imaging

Harvested cells were immunolabeled with CD4- and CD8-targeting antibodies (BD, **Table S2**) prior to in fixation in 4% paraformaldehyde (ThermoFisher, Waltham, MA) diluted in PBS for 15 minutes at ambient temperature and immobilized onto 1.5H coverslips (Thor Labs, Newton, NJ) by centrifugation on a Cytospin 4 cytocentrifuge (Eprelia, Kalamazoo, MI). Coverslips were placed in 35 mm dishes for subsequent cell permeabilization in 1% Triton-X 100 (MilliporeSigma, Burlington, MA) and intracellular immunolabeling with anti-TOM20 primary antibody (Cell Signaling Technology, Danvers, MA) and Alexa Fluor® 647 conjugated anti-Rabbit IgG (Cell Signaling Technology). Coverslips were mounted onto glass slides (ThermoFisher) using ProLong Glass antifade mountant (ThermoFisher, Waltham, MA), sealed with clear nail polish, and allowed to dry in the dark at ambient temperature for ~24hrs. Slides were imaged on a DeltaVision OMX Super-Resolution SIM microscope on the widefield setting using an 80x objective with $n = 1.516$ immersion oil. Single T cells were imaged in serial sections along the z-axis such that stacks of ≥ 20 images were collected per cell. Images were deconvoluted using SoftWoRx software (Cytiva, Marlborough, MA). Deconvoluted image stacks were reconstructed as 3D projections using Imaris software

(Oxford Instruments, Abingdon, United Kingdom) and mitochondrial volume was determined from masked projections. Volume measurements were plotted and statistical analysis was performed on Prism software (GraphPad, La Jolla, CA).

Statistical analysis

Statistical analyses were conducted using Prism version 8 (GraphPad, La Jolla, CA). Statistical significance was determined using two-tailed student's t-tests for two-way comparisons and 2-way analysis of variation (ANOVA) for multiple comparisons. For all statistical analyses, a p-value <0.05 were considered significant.

Protocol 1: Mitochondrial Mass and Membrane Potential Staining for Human Lymphocytes

By Kevin Z. Chen

1. Reagents
 - a. Phenol red and serum free media (ThermoFisher, No. 11835030)
 - b. Staining media (BioLegend, No. 420201)
 - c. MitoTracker Dyes (ThermoFisher, **Table S2**)
 - d. TMRM (ThermoFisher, No. T668)
 - e. CCCP (Millipore Sigma# C2759-100MG)
2. Preparation of Mito. Dye Solutions
 - a. Prepare 50uM of MitoTracker Green FM (mass)
 - b. Prepare 50uM of MitoTracker Deep Red (membrane potential), MitoTracker Orange CM(H₂)TMRos (active ETC/OXPHOS and membrane potential), MitoTracker Orange CMTMRos (membrane potential), or TMRM (membrane potential)
 - i. MitoTracker Green FM and TMRM cannot be fixed, others can be fixed but signal typically is reduced after fixation
 - ii. At high concentrations above ~150-200nM, MitoTracker Green FM starts to stain other cellular structures and organelles.
 - c. Dilute MitoTrackers 1:1000 in warmed *serum free* media (i.e. RPMI-1640 alone) for a final concentration of 50nM
 - i. MitoTrackers are sensitive to oxidases in serum so do not use PBS + 2% FBS or complete medium
 - ii. If using TMRM, dilute 50uM TMRM stock 1:500 in warmed *serum free* media for 100nM
3. Live Cell Staining
 - a. Add 500uL of 50nM MitoTracker Green FM and 500uL of 50nM MitoTracker Deep Red or equivalent for every 1e6 live cells for a final suspension of 25nM/25nM MitoTracker Green FM/Deep Red
 - i. If using only MitoTracker Green FM or Deep Red, then diluted further to 25nM and add 1mL of 25nM mito. dye to 1e6 live cells
 - b. Place cells in 37C incubator for 15 minutes in non-sterile incubator
 - i. Protect from light
 - ii. If signal is too strong, stain for 10-12 minutes
 - c. Wash twice in *phenol red and serum free* media (vortex in wash → centrifuge for 5 minutes at 300g → decant supernatant) and resuspend in appropriate buffer or medium
 - i. For the last wash steps and resuspension, staining media or PBS + 2% FBS is fine as well. Just be sure to run the samples immediately afterwards to avoid cell death or dye oxidation.
 1. Note: Staining media contains NaN₃ which is a metabolic inhibitor so try to reduce the time cells stay in staining media prior to flow acquisition
 - d. Note: When cells start to die, mitochondrial membrane potential dyes will quickly dissipate and signal will drastically decline
4. Flow Cytometry on Cytex Aurora Cytometer
 - a. Be sure to include appropriate compensation controls. MitoTrackers only stain live cells so OneComp eBeads cannot be used for compensation controls.
 - i. For mitochondrial membrane potential, treat cells with CCCP, camptothecin, or kill a portion of cells prior to staining to use as an appropriate negative control.
 - b. When running, be sure to check the appropriate channels to make sure signal is within range (fluorescent intensity < 10⁶). Adjust the laser voltage if necessary.

Protocol 2: Immunoblot/Western Blot Protocol*

By Kevin Z. Chen

*In this protocol, I have used phosphor-S437-AKT antibody (CST, 4060S) as an example

1. Cell lysate prep
 - a. Harvest 5e6-10e6 T cells
 - b. Centrifuge cells suspension at 1500 rpm for 5 min to separate and remove media
 - c. Aspirate media
 - d. Wash with 1x cold PBS
 - e. Resuspend cells in 50-100 uL of RIPA plus 10x phosphatase inhibitors (Millipore Sigma, P2850-5ML) and 10x protease inhibitors (Millipore Sigma, P8340-5ML)
 - i. I usually freshly add 100 uL protease inhibitors and 20 uL phosphatase inhibitors for 1 mL total solution in RIPA right before use
 - ii. I use ~50uL of RIPA/inhibitors solution for 10uL of pellet or 5e6 T cells, I would not try to lyse < 5e6 T cells due to insufficient protein yield
 - f. Vortex well
 - g. Shake for 15-20 min on ice
 - h. Centrifuge for 20 min at max speed
2. WB sample prep
 - a. Conduct Bradford Assay
 - b. Dilute protein lysate with RIPA plus inhibitors (doesn't need to be fresh) to load at least 30 ug protein per well
 - c. Make final WB sample with appropriate amount of 6x loading buffer (Fischer Scientific, AAJ61337AC)
3. Electrophoresis
 - a. Run the gel at 180V for ~30-40 min depending on the gel composition.
 - b. Running the gel at 200V for 30 minutes as recommended by Bio-Rad sometimes causes strange banding patterns and curvature.
4. Transfer
 - a. Follow Bio-Rad Transblot Turbo Semi-Dry Transfer protocol
 - i. Wet transfer should be fine as well, especially for high kDa proteins
 - ii. Note: If using Bio-Rad Semi-Dry Transfer system, ONLY use the associated Bio-Rad Turbo products and transfer buffer
5. Blocking
 - a. Block membrane in 1% BSA made from 10x Blocker BSA stock (Thermo Scientific, 37525) for 1-2 hour at RT in a black membrane box to protect membrane from light
 - i. I reuse or discard blocking solution depending on if I had stripped the membrane but for p.AKT this will have been the first thing I probed for
6. Primary antibody
 - a. Use 1:500 – 1:1000 p.AKT antibody (CST, 4060S) in 1% BSA
 - i. Either add primary antibody directly to blocking solution in box with membrane or prepare separately
 - b. Incubate primary antibody with membrane with shaking at 4C overnight
 - c. Next day, acclimate the membrane to RT with shaking for one hour to allow for last minute binding
 - d. Store antibody for reuse
 - e. Wash membrane in 1x TBS-Tween20 (1%) for 10 minutes on shaker 3 times
7. Secondary antibody
 - a. Use 1:5000 goat anti-rabbit HRP-conjugated (Abcam, ab205718) in 1% BSA in TBS-Tween20

- b. Incubate secondary antibody with membrane with shaking at RT for ~1 hr
 - c. Wash membrane in 1x TBS-Tween20 (1%) for 15 minutes on shaker 3 times
8. Imaging
- a. Image using SuperSignal West Pico PLUS Chemiluminescent Substrate (Thermo Scientific, 34580) and Azure Biosystems Imager on Chemiluminescent setting (Winship Shared Resources, Building B, 5th Floor)

Works Cited

1. Funk CR, Wang S, Chen KZ, Waller A, Sharma A, Edgar CL, Gupta VA, Chandrakasan S, Zoine JT, Fedanov A, Raikar SS, Koff JL, Flowers CR, Coma S, Pachter JA, Ravindranathan S, Spencer HT, Shanmugam M, Waller EK. PI3K δ/γ inhibition promotes human CART cell epigenetic and metabolic reprogramming to enhance antitumor cytotoxicity. *Blood*. 2022;139(4):523-37. doi: 10.1182/blood.2021011597.
2. Biel TG, Lee S, Flores-Toro JA, Dean JW, Go KL, Lee MH, Law BK, Law ME, Dunn WA, Zendejas I, Behrns KE, Kim JS. Sirtuin 1 suppresses mitochondrial dysfunction of ischemic mouse livers in a mitofusin 2-dependent manner. *Cell Death & Differentiation*. 2016;23(2):279-90. doi: 10.1038/cdd.2015.96.
3. Meng H, Yan W-Y, Lei Y-H, Wan Z, Hou Y-Y, Sun L-K, Zhou J-P. SIRT3 Regulation of Mitochondrial Quality Control in Neurodegenerative Diseases. *Frontiers in Aging Neuroscience*. 2019;11. doi: 10.3389/fnagi.2019.00313.
4. Oanh NTK, Park Y-Y, Cho H. Mitochondria elongation is mediated through SIRT1-mediated MFN1 stabilization. *Cellular Signalling*. 2017;38:67-75. doi: <https://doi.org/10.1016/j.cellsig.2017.06.019>.

5. Shen L, Zhang Q, Tu S, Qin W. SIRT3 mediates mitofusin 2 ubiquitination and degradation to suppress ischemia reperfusion-induced acute kidney injury. *Experimental Cell Research*. 2021;408(2):112861-undefined. doi: 10.1016/j.yexcr.2021.112861.
6. Tseng AHH, Shieh S-S, Wang DL. SIRT3 deacetylates FOXO3 to protect mitochondria against oxidative damage. *Free Radical Biology and Medicine*. 2013;63:222-34. doi: <https://doi.org/10.1016/j.freeradbiomed.2013.05.002>.
7. Anderson MA, Tam C, Lew TE, Juneja S, Juneja M, Westerman D, Wall M, Lade S, Gorelik A, Huang DCS, Seymour JF, Roberts AW. Clinicopathological features and outcomes of progression of CLL on the BCL2 inhibitor venetoclax. *Blood*. 2017;129(25):3362-70. doi: 10.1182/blood-2017-01-763003.
8. O'Brien S, Furman RR, Coutre S, Flinn IW, Burger JA, Blum K, Sharman J, Wierda W, Jones J, Zhao W, Heerema NA, Johnson AJ, Luan Y, James DF, Chu AD, Byrd JC. Single-agent ibrutinib in treatment-naïve and relapsed/refractory chronic lymphocytic leukemia: a 5-year experience. *Blood*. 2018;131(17):1910-9. doi: 10.1182/blood-2017-10-810044.
9. Mato AR, Thompson MC, Nabhan C, Svoboda J, Schuster SJ. Chimeric Antigen Receptor T-Cell Therapy for Chronic Lymphocytic Leukemia: A Narrative Review. *Clinical Lymphoma Myeloma and Leukemia*. 2017;17(12):852-6. doi: 10.1016/j.clml.2017.07.007.
10. Gribben JG. How and when I do allogeneic transplant in CLL. *Blood*. 2018;132(1):31-9. doi: 10.1182/blood-2018-01-785998.
11. Chavez JC, Bachmeier C, Kharfan-Dabaja MA. CAR T-cell therapy for B-cell lymphomas: clinical trial results of available products. *Ther Adv Hematol*. 2019;10:2040620719841581-. doi: 10.1177/2040620719841581. PubMed PMID: 31019670.
12. Abramson J, Palomba M, Gordon L, Lunning M, Wang M, Arnason J, Mehta A, Purev E, Maloney D, Andreadis C, Sehgal A, Solomon S, Ghosh N, Albertson T, Garcia J, Kostic A, Mallaney M, Ogasawara K, Newhall K, Kim Y, Li D, Siddiqi T. Lisocabtagene maraleucel for patients with relapsed or refractory large B-cell lymphomas (TRANSCEND NHL 001): a multicentre seamless design study. *The Lancet*. 2020;396(10254):839-52. doi: 10.1016/S0140-6736(20)31366-0.
13. Neelapu SS, Locke FL, Bartlett NL, Lekakis LJ, Miklos DB, Jacobson CA, Braunschweig I, Oluwole OO, Siddiqi T, Lin Y, Timmerman JM, Stiff PJ, Friedberg JW, Flinn IW, Goy A, Hill BT, Smith MR, Deol A, Farooq U, McSweeney P, Munoz J, Avivi I, Castro JE, Westin JR, Chavez JC, Ghobadi A, Komanduri KV, Levy R, Jacobsen ED, Witzig TE, Reagan P, Bot A, Rossi J, Navale L, Jiang Y, Aycocck J, Elias M, Chang D, Wiecek J, Go WY. Axicabtagene Ciloleucel CAR T-Cell Therapy in Refractory Large B-Cell Lymphoma. *N Engl J Med*. 2017;377(26):2531-44. Epub 2017/12/10. doi: 10.1056/NEJMoa1707447. PubMed PMID: 29226797.
14. Schuster SJ, Bishop MR, Tam CS, Waller EK, Borchmann P, McGuirk JP, Jäger U, Jaglowski S, Andreadis C, Westin JR, Fleury I, Bachanova V, Foley SR, Ho PJ, Mielke S, Magenau JM, Holte H, Pantano S, Pacaud LB, Awasthi R, Chu J, Anak Ö, Salles G, Maziarz RT. Tisagenlecleucel in Adult Relapsed or Refractory Diffuse Large B-Cell Lymphoma. *New England Journal of Medicine*. 2019;380(1):45-56. doi: 10.1056/nejmoa1804980.
15. Mian A, Hill BT. Brexucabtagene autoleucel for the treatment of relapsed/refractory mantle cell lymphoma. *Expert Opinion on Biological Therapy*. 2021:1-7. doi: 10.1080/14712598.2021.1889510.
16. Ventola CL. Cancer Immunotherapy, Part 2: Efficacy, Safety, and Other Clinical Considerations. *P T*. 2017;42(7):452-63. PubMed PMID: 28674473.
17. Guedan S, Ruella M, June CH. Emerging Cellular Therapies for Cancer. *Annual Review of Immunology*. 2018;37(1):145-71. doi: 10.1146/annurev-immunol-042718-041407.
18. Wagner J, Wickman E, Derenzo C, Gottschalk S. CAR T Cell Therapy for Solid Tumors: Bright Future or Dark Reality? *Molecular Therapy*. 2020;28(11):2320-39. doi: 10.1016/j.ymthe.2020.09.015.
19. Xu X, Sun Q, Liang X, Chen Z, Zhang X, Zhou X, Li M, Tu H, Liu Y, Tu S, Li Y. Mechanisms of Relapse After CD19 CAR T-Cell Therapy for Acute Lymphoblastic Leukemia and Its Prevention and Treatment Strategies. *Frontiers in Immunology*. 2019;10.

20. Fraietta JA, Lacey SF, Orlando EJ, Pruteanu-Malinici I, Gohil M, Lundh S, Boesteanu AC, Wang Y, O'Connor RS, Hwang W-T, Pequignot E, Ambrose DE, Zhang C, Wilcox N, Bedoya F, Dorfmeier C, Chen F, Tian L, Parakandi H, Gupta M, Young RM, Johnson FB, Kulikovskaya I, Liu L, Xu J, Kassim SH, Davis MM, Levine BL, Frey NV, Siegel DL, Huang AC, Wherry EJ, Bitter H, Brogdon JL, Porter DL, June CH, Melenhorst JJ. Determinants of response and resistance to CD19 chimeric antigen receptor (CAR) T cell therapy of chronic lymphocytic leukemia. *Nat Med.* 2018;24(5):563-71. doi: 10.1038/s41591-018-0010-1.
21. Ana, Joller N, Vijay. Lag-3, Tim-3, and TIGIT: Co-inhibitory Receptors with Specialized Functions in Immune Regulation. *Immunity.* 2016;44(5):989-1004. doi: 10.1016/j.immuni.2016.05.001.
22. Datar I, Sanmamed MF, Wang J, Henick BS, Choi J, Badri T, Dong W, Mani N, Toki M, Mejías LD, Lozano MD, Perez-Gracia JL, Velcheti V, Hellmann MD, Gainor JF, McEachern K, Jenkins D, Syrigos K, Politi K, Gettinger S, Rimm DL, Herbst RS, Melero I, Chen L, Schalper KA. Expression Analysis and Significance of PD-1, LAG-3, and TIM-3 in Human Non-Small Cell Lung Cancer Using Spatially Resolved and Multiparametric Single-Cell Analysis. *Clinical Cancer Research.* 2019;25(15):4663-73. doi: 10.1158/1078-0432.ccr-18-4142.
23. Sakuishi K, Apetoh L, Sullivan JM, Blazar BR, Kuchroo VK, Anderson AC. Targeting Tim-3 and PD-1 pathways to reverse T cell exhaustion and restore anti-tumor immunity. *Journal of Experimental Medicine.* 2010;207(10):2187-94. doi: 10.1084/jem.20100643.
24. Buck MD, O'Sullivan D, Klein Geltink RI, Curtis JD, Chang C-H, Sanin DE, Qiu J, Kretz O, Braas D, van der Windt GJW, Chen Q, Huang SC-C, O'Neill CM, Edelson BT, Pearce EJ, Sesaki H, Huber TB, Rambold AS, Pearce EL. Mitochondrial Dynamics Controls T Cell Fate through Metabolic Programming. *Cell.* 2016;166(1):63-76. Epub 2016/06/09. doi: 10.1016/j.cell.2016.05.035. PubMed PMID: 27293185.
25. Lanna A, Dustin ML. Mitochondrial fusion fuels T cell memory. *Cell Res.* 2016;26(9):969-70. Epub 2016/08/12. doi: 10.1038/cr.2016.94. PubMed PMID: 27514702.
26. Patten DA, Wong J, Khacho M, Soubannier V, Mailloux RJ, Pilon-Larose K, Maclaurin JG, Park DS, McBride HM, Trinkle-Mulcahy L, Harper ME, Germain M, Slack RS. OPA1-dependent cristae modulation is essential for cellular adaptation to metabolic demand. *The EMBO Journal.* 2014;33(22):2676-91. doi: 10.15252/embj.201488349.
27. Luchsinger LL, de Almeida MJ, Corrigan DJ, Mumau M, Snoeck H-W. Mitofusin 2 maintains haematopoietic stem cells with extensive lymphoid potential. *Nature.* 2016;529(7587):528-31. doi: 10.1038/nature16500.
28. Zhao G-j, Yao Y-m, Lu Z-q, Hong G-l, Zhu X-m, Wu Y, Wang D-w, Dong N, Yu Y, Sheng Z-y. Up-regulation of mitofusin-2 protects CD4+ T cells from HMGB1-mediated immune dysfunction partly through Ca²⁺-NFAT signaling pathway. *Cytokine.* 2012;59(1):79-85. doi: <https://doi.org/10.1016/j.cyto.2012.03.026>.
29. Lu Z-q, Tang L-m, Zhao G-j, Yao Y-m, Zhu X-m, Dong N, Yu Y. Overactivation of Mitogen-Activated Protein Kinase and Suppression of Mitofusin-2 Expression Are Two Independent Events in High Mobility Group Box 1 Protein-Mediated T Cell Immune Dysfunction. *Journal of Interferon & Cytokine Research.* 2013;33(9):529-41. doi: 10.1089/jir.2012.0054.
30. Schrepfer E, Scorrano L. Mitofusins, from Mitochondria to Metabolism. *Molecular Cell.* 2016;61(5):683-94. doi: 10.1016/j.molcel.2016.02.022.
31. Qi Y, Yan L, Yu C, Guo X, Zhou X, Hu X, Huang X, Rao Z, Lou Z, Hu J. Structures of human mitofusin 1 provide insight into mitochondrial tethering. *Journal of Cell Biology.* 2016;215(5):621-9. doi: 10.1083/jcb.201609019.
32. Koshiba T, Detmer Scott A, Kaiser Jens T, Chen H, McCaffery JM, Chan David C. Structural Basis of Mitochondrial Tethering by Mitofusin Complexes. *Science.* 2004;305(5685):858-62. doi: 10.1126/science.1099793.
33. Leonard AP, Cameron RB, Speiser JL, Wolf BJ, Peterson YK, Schnellmann RG, Beeson CC, Rohrer B. Quantitative analysis of mitochondrial morphology and membrane potential in living cells

using high-content imaging, machine learning, and morphological binning. *Biochimica et Biophysica Acta (BBA) - Molecular Cell Research*. 2015;1853(2):348-60. doi:

<https://doi.org/10.1016/j.bbamcr.2014.11.002>.

34. Cipolat S, de Brito Olga M, Dal Zilio B, Scorrano L. OPA1 requires mitofusin 1 to promote mitochondrial fusion. *Proceedings of the National Academy of Sciences*. 2004;101(45):15927-32. doi: 10.1073/pnas.0407043101.
35. Zacharioudakis E, Agianian B, Kumar Mv V, Biris N, Garner TP, Rabinovich-Nikitin I, Ouchida AT, Margulets V, Nordstrøm LU, Riley JS, Dolgalev I, Chen Y, Wittig AJH, Pekson R, Mathew C, Wei P, Tsirigos A, Tait SWG, Kirshenbaum LA, Kitsis RN, Gavathiotis E. Modulating mitofusins to control mitochondrial function and signaling. *Nature Communications*. 2022;13(1):3775. doi: 10.1038/s41467-022-31324-1.
36. Klein Geltink RI, Kyle RL, Pearce EL. Unraveling the Complex Interplay Between T Cell Metabolism and Function. *Annual Review of Immunology*. 2018;36(1):461-88. doi: 10.1146/annurev-immunol-042617-053019.
37. Song Z, Ghochani M, McCaffery JM, Frey TG, Chan DC. Mitofusins and OPA1 Mediate Sequential Steps in Mitochondrial Membrane Fusion. *Molecular Biology of the Cell*. 2009;20(15):3525-32. doi: 10.1091/mbc.e09-03-0252.
38. Ge Y, Shi X, Boopathy S, McDonald J, Smith AW, Chao LH. Two forms of Opal cooperate to complete fusion of the mitochondrial inner-membrane. *eLife*. 2020;9:e50973. doi: 10.7554/eLife.50973.
39. Cartoni R, Léger B, Hock MB, Praz M, Crettenand A, Pich S, Ziltener J-L, Luthi F, Dériaz O, Zorzano A, Gobelet C, Kralli A, Russell AP. Mitofusins 1/2 and ERR α expression are increased in human skeletal muscle after physical exercise. *The Journal of Physiology*. 2005;567(1):349-58. doi: <https://doi.org/10.1113/jphysiol.2005.092031>.
40. Panes JD, Godoy PA, Silva-Grecchi T, Celis MT, Ramirez-Molina O, Gavilan J, Muñoz-Montecino C, Castro PA, Moraga-Cid G, Yévenes GE, Guzmán L, Salisbury JL, Trushina E, Fuentealba J. Changes in PGC-1 α /SIRT1 Signaling Impact on Mitochondrial Homeostasis in Amyloid-Beta Peptide Toxicity Model. *Frontiers in Pharmacology*. 2020;11.
41. Martin OJ, Lai L, Soundarapandian MM, Leone TC, Zorzano A, Keller MP, Attie AD, Muoio DM, Kelly DP. A Role for Peroxisome Proliferator-Activated Receptor γ Coactivator-1 in the Control of Mitochondrial Dynamics During Postnatal Cardiac Growth. *Circulation Research*. 2014;114(4):626-36. doi: 10.1161/CIRCRESAHA.114.302562.
42. Pillai VB, Kanwal A, Fang YH, Sharp WW, Samant S, Arbiser J, Gupta MP. Honokiol, an activator of Sirtuin-3 (SIRT3) preserves mitochondria and protects the heart from doxorubicin-induced cardiomyopathy in mice. *Oncotarget*. 2017;8(21):34082-98. doi: 10.18632/oncotarget.16133.
43. Dasgupta A, Chen K-H, Munk RB, Sasaki CY, Curtis J, Longo DL, Ghosh P. Mechanism of Activation-Induced Downregulation of Mitofusin 2 in Human Peripheral Blood T Cells. *The Journal of Immunology*. 2015;195(12):5780. doi: 10.4049/jimmunol.1501023.
44. Chao T, Wang H, Ho P-C. Mitochondrial Control and Guidance of Cellular Activities of T Cells. *Frontiers in Immunology*. 2017;8.
45. Quintana A, Schwindling C, Wenning AS, Becherer U, Rettig J, Schwarz EC, Hoth M. T cell activation requires mitochondrial translocation to the immunological synapse. *Proceedings of the National Academy of Sciences*. 2007;104(36):14418-23. doi: 10.1073/pnas.0703126104.
46. Priault M, Salin B, Schaeffer J, Vallette FM, di Rago JP, Martinou JC. Impairing the bioenergetic status and the biogenesis of mitochondria triggers mitophagy in yeast. *Cell Death & Differentiation*. 2005;12(12):1613-21. doi: 10.1038/sj.cdd.4401697.
47. Twig G, Shirihai OS. The Interplay Between Mitochondrial Dynamics and Mitophagy. *Antioxidants & Redox Signaling*. 2011;14(10):1939-51. doi: 10.1089/ars.2010.3779.
48. Twig G, Elorza A, Molina AJA, Mohamed H, Wikstrom JD, Walzer G, Stiles L, Haigh SE, Katz S, Las G, Alroy J, Wu M, Py BF, Yuan J, Deeney JT, Corkey BE, Shirihai OS. Fission and selective

- fusion govern mitochondrial segregation and elimination by autophagy. *The EMBO Journal*. 2008;27(2):433-46. doi: 10.1038/sj.emboj.7601963.
49. Legros F, Lombès A, Frachon P, Rojo M. Mitochondrial Fusion in Human Cells Is Efficient, Requires the Inner Membrane Potential, and Is Mediated by Mitofusins. *Molecular Biology of the Cell*. 2002;13(12):4343-54. doi: 10.1091/mbc.e02-06-0330.
50. Dong F, Zhu M, Zheng F, Fu C. Mitochondrial fusion and fission are required for proper mitochondrial function and cell proliferation in fission yeast. *The FEBS Journal*. 2022;289(1):262-78. doi: 10.1111/febs.16138.
51. Lugli E, Troiano L, Ferraresi R, Roat E, Prada N, Nasi M, Pinti M, Cooper EL, Cossarizza A. Characterization of cells with different mitochondrial membrane potential during apoptosis. *Cytometry Part A*. 2005;68A(1):28-35. doi: 10.1002/cyto.a.20188.
52. Xiao B, Deng X, Zhou W, Tan E-K. Flow Cytometry-Based Assessment of Mitophagy Using MitoTracker. *Frontiers in Cellular Neuroscience*. 2016;10.
53. Jones N, Cronin JG, Dolton G, Panetti S, Schauenburg AJ, Galloway SAE, Sewell AK, Cole DK, Thornton CA, Francis NJ. Metabolic Adaptation of Human CD4+ and CD8+ T-Cells to T-Cell Receptor-Mediated Stimulation. *Frontiers in Immunology*. 2017;8.
54. Youle RJ, Narendra DP. Mechanisms of mitophagy. *Nature Reviews Molecular Cell Biology*. 2011;12(1):9-14. doi: 10.1038/nrm3028.
55. Tanida I, Ueno T, Kominami E. LC3 and Autophagy. Humana Press; 2008. p. 77-88.
56. da Silva Rosa SC, Martens MD, Field JT, Nguyen L, Kereliuk SM, Hai Y, Chapman D, Diehl-Jones W, Aliani M, West AR, Thliveris J, Ghavami S, Rampitsch C, Dolinsky VW, Gordon JW. BNIP3L/Nix-induced mitochondrial fission, mitophagy, and impaired myocyte glucose uptake are abrogated by PRKA/PKA phosphorylation. *Autophagy*. 2021;17(9):2257-72. doi: 10.1080/15548627.2020.1821548.
57. Kubli Dieter A, Ycaza John E, Gustafsson Åsa B. Bnip3 mediates mitochondrial dysfunction and cell death through Bax and Bak. *Biochemical Journal*. 2007;405(3):407-15. doi: 10.1042/BJ20070319.
58. Clinical Trials Involving Duvelisib: National Institutes of Health; 2022 [July 29, 2022] Search results for "duvelisib". Available from: <https://clinicaltrials.gov/ct2/results?cond=&term=duvelisib&cntry=&state=&city=&dist=&Search=Search>.
59. Roth L. Secura Bio, Inc.; Withdrawal of Approval of Relapsed or Refractory Follicular Lymphoma Indication for COPIKTRA [Public Notice]. Federal Register: Food and Drug Administration, HHS; 2022 [cited 2022 July 29].
60. Chen KZ, Funk CR, Wang S, Sharma A, Waller EK, Shanmugam M. Duvelisib Promotes Mitochondrial Fusion and Epigenetic Reprogramming to Drive Therapeutic T Cell Persistence and Function. *Blood*. 2021;138(Supplement 1):1714-. doi: 10.1182/blood-2021-153446.
61. Chazotte B. Labeling mitochondria with MitoTracker dyes. *Cold Spring Harb Protoc*. 2011;2011(8):990-2. Epub 20110801. doi: 10.1101/pdb.prot5648. PubMed PMID: 21807856.
62. Chang C-H, Curtis Jonathan D, Maggi Leonard B, Jr., Faubert B, Villarino Alejandro V, O'Sullivan D, Huang Stanley C-C, van der Windt Gerritje JW, Blagih J, Qiu J, Weber Jason D, Pearce Edward J, Jones Russell G, Pearce Erika L. Posttranscriptional Control of T Cell Effector Function by Aerobic Glycolysis. *Cell*. 2013;153(6):1239-51. doi: 10.1016/j.cell.2013.05.016.